Behavior of Overdeformed Shield Tunnel Lining under Grouting Treatment: Field Experiment

Citation for published version:
Han, T, Wu, G, Lu, Y, Yu, B & Gao, Y 2021, 'Behavior of Overdeformed Shield Tunnel Lining under Grouting Treatment: Field Experiment', *Journal of Performance of Constructed Facilities*, vol. 35, no. 6, 04021082, pp. 1. https://doi.org/10.1061/(ASCE)CF.1943-5509.0001657

Digital Object Identifier (DOI):
10.1061/(ASCE)CF.1943-5509.0001657

Published In:
Journal of Performance of Constructed Facilities

Behavior of Over-Deformed Shield Tunnel Lining under Grouting Treatment: Field Experiment

Tianran Han [1] ; Gang Wu [2]; Yong Lu [3] ; Baiyong Yu [4] ; and Yong Gao [5]

[1]Ph.D. Candidate, Key Laboratory of Concrete and Prestressed Concrete Structures of the Ministry of Education, Southeast University, Nanjing 211189, China; National and Local Joint Engineering Research Center for Intelligent Construction and Maintenance, Nanjing 211189, China. Email: tianran.han@hotmail.com

[2]Professor, Key Laboratory of Concrete and Prestressed Concrete Structures of the Ministry of Education, Southeast University, Nanjing 211189, China; National and Local Joint Engineering Research Center for Intelligent Construction and Maintenance, Nanjing 211189, China(corresponding author). Email: g.wu@seu.edu.cn

[3]Professor, Institute for Infrastructure and Environment, School of Engineering, The University of Edinburgh, Edinburgh EH9 3JL, UK. Email: Yong.Lu@ed.ac.uk

[4]Senior Engineer, Nanjing Metro Group Co., Ltd, Nanjing 210008, China. Email: yu_by@njmetro.com.cn

[5]Civil Engineer, Nanjing Metro Operation Co., Ltd, Nanjing 210046, China. Email: gaoyong_820311@163.com

---

Abstract:

Shield tunnel structures are commonly found to be over-deformed in Eastern China soft ground due to adjacent engineering activities. Grouting treatment could serve as a viable solution to reduce the excessive diametrical expansion of tunnel linings actively. However, understanding the grouting-induced effects on adjacent tunnel structures remains preliminary due to the scarcity of well-documented case histories. In this study, a field experiment was conducted to explore a shield metro tunnel's real performance during grouting treatments. An extensive monitoring scheme was deployed while varied geometrical grouting arrangements were carried out. The tests provided a comprehensive database of the tunnel responses in multiple temporal resolution levels, both during the entire course of the grouting treatment and within single grouting operations. Investigations are carried out over the influencing factors of the grouting efficiency. The experimental observations suggest that grouting efficiency tends to evolve with time and can be affected by various geometrical grouting parameters. Observations are also presented and discussed in detail for the influence of grouting history on the convergence distribution and the tunnel's performance after the termination of all grouting operations.

Time-variant behaviors of the tunnel are depicted in detail, such as the convergence recovery and rebound during the grouting process. Overall, this case study brings new insights into understanding the grouting-induced tunnel lining response. It can also serve as a benchmark for further theoretical and numerical studies.

Author keywords: Field experiment; Shield tunnel structure; Real performance; Grouting treatment; Deformation mitigation

---

Introduction

Recent years have seen a massive development of metro networks in major cities worldwide as an efficient way to enhance urban transit capabilities and alleviate the stress of traffic congestions (Shen, et al., 2014). It also helps promote further development of the urban area, bringing more buildings to be constructed along the metro corridors. As a result, more engineering operations tend to occur adjacent to the metro tunnels. Segmental shield tunnel established in soft grounds can be especially problematic and is frequently observed to suffer from excessive deformation due to the weak strength of soil or environmental changes (Shen, et al., 2014).

Due to the adjacent engineering activities, such as deep excavations (Chang, et al., 2001, Chen, et al., 2016, Cheng, et al., 2018, Huang, et al., 2013, Li, et al., 2017, Liu, et al., 2016, Tan, et al., 2015), tunneling (Cooper, et al., 2002, Mohamad, et al., 2012), or extreme surcharges (Huang and Zhang, 2016, Huang, et al., 2017), the current tunnel structures can be further distorted, which can adversely impact the integrity of the structures. For example, because of the excavation of the Shell Center project, the Bakerloo metro line beneath the excavation experienced a heave motion by 50 mm in a 27-year time period (Burford, 1988). In Taipei, a portion of the shield tunnel in the Panchiao Line was over-deformed and damaged because of nearby excavation. Cracks were found in the reinforced concrete segments, and the concrete slab on the tunnel invert was displaced (Chang, et al., 2001). Due to the influence of the adjacent excavation, a tunnel section in Ningbo Metro Line 1 reached a horizontal displacement of 33.5 mm, with cracks and leakages appearing in the left-line tunnel (Chen, et al., 2016). In Zhengzhou, a similar case was reported concerning the impact of excavations on the existing tunnel, and the cumulative uplift and lateral displacement of the tunnel was measured to reach

22.9 mm and 77.9 mm, respectively, as the excavations progressed to their final depth (Cheng, et al., 2018). In London, the construction of three station tunnels at the Heathrow Express Central Terminal was reported to create an additional settlement, distortion, and rotation movement to the Piccadilly Line tunnel. Subsequently, compensation grouting was undertaken to achieve settlement mitigation (Cooper, et al., 2002). Similarly, an operating shield metro tunnel in Shanghai, China, was reported to be heavily disrupted by an unexpected extreme surcharge (Huang and Zhang, 2016, Huang, et al., 2017).

Among the potential impacts from the adjacent engineering activities, the large circumferential deformation of the tunnel is the one that arouses the gravest safety concern. For the circumferential deformation, the increase in the tunnel's horizontal diameter (horizontal convergence, ΔD, as illustrated in Fig.3), is usually adopted as the key performance indicator (Liu, et al., 2016, Mair, 2008, Pinto and Whittle, 2014). In some soft ground cases, the tunnel convergence was reported to nearly reach the level of the ultimate bearing capacity of the segmental linings (Liu, et al., 2016). Excessive tunnel convergence can result in structural issues such as spalling, cracking, leakages, and segment dislocation (Huang, et al., 2013, Shi and Li, 2015). Therefore, effective mitigation measures are imperative to maintain the safety and sustainability of tunnel structures (Han, et al., 2020).

In recent years, various methods to tackle these problems have been developed in engineering practice. Reinforcement measures using aramid fiber-reinforced polymer (AFRP) reinforcement (Huang and Zhang, 2016, Huang, et al., 2017) and bonded steel plates are the most commonly used methods from the structural strengthening point of view (Ai, et al., 2017, Chang, et al., 2001, Kiriyama, et al., 2005, Zhao, et al., 2016). However, these passive control measures cannot alleviate the deformation that already occurred. Besides, the work can only be carried out in the mid-night hours if significant disruption to the metro service is to be avoided, leading to reduced construction efficiency.

Differing from the passive reinforcement-type deformational control approaches, treatment methods based on grouting introduce control mechanisms to actively restore the excessively deformed lining rings to an acceptable level. Traditionally, compensation grouting has been used worldwide for deformational control of geo-structures and the ground (Farrell, 2015, Komiya, et al., 2001, Lee, 2002). However, the grouting operations may generate substantial disturbance to the surrounding soil, especially when the ground consists of sensitive soft deposits.

A grouting-based technique has recently been developed to achieve minimal disturbance to the surrounding soil (Zhang, et al., 2018). The technique adopts a dual-fluid system with the use of associated innovative grouting equipment. Fast-setting grout is injected into the soil during the grouting treatment, creating a soil-concrete mixture with improved ground resistance to the deformational movements of tunnel linings (Zhi-jun, 2011). In the meantime, the treatment also creates counter-pressure against the imbalanced pressure induced by neighboring engineering operations. Successful implementations of this technique have been reported from a number of grouting projects, especially in soft soil areas in Eastern China (Huang and Zhang, 2016, Jin, et al., 2018, Li and Chen, 2012, Li and Yuan, 2016, Zhang, et al., 2018, Zhou, et al., 2018, Zhu, et al., 2019). The grouting technique proved to be effective in the mitigation of excessive deformation for tunnels, both longitudinally and circumferentially. For instance, for the longitudinal deformational control, a reduction in the settlement rate and uplifting of the tunnel back to a safe state were achieved in Shanghai-based projects (Zhang, et al., 2018). Elsewhere, the technique was used to achieve active control for the excessive horizontal displacement of the tunnel due to nearby excavations (Zheng, et al., 2020). Similarly, the technique was applied to rehabilitate a circumferentially over-deformed tunnel due to extreme surcharges, and on average, 25% of the original large convergence reduction was attained (Zhang, et al., 2019). Although these reported case histories illustrate the effectiveness of the grouting technique, they tend to focus on the total effects of the deformational control rather than detailed observation of the temporal and spatial evolution of the tunnel structural response. From this point of view, further investigation is still needed to provide insights into the real performance of tunnels under the effects of grouting.

This paper describes a full-scale field experiment of grouting treatment based in Eastern China soft ground. The experiment provides detailed observations from varied grouting arrangements, which were designed in an attempt to reduce existing tunnel convergence. A systematic investigation is conducted into various effects of grouting operations and their influencing factors, such as the time-variant response of tunnel linings, effects of grouting history, influencing factors of grouting efficiency, and characteristics of the tunnel lining rebounding after grouting. The study provides new insights into the understanding of the grouting-induced tunnel lining responses, and it also provides benchmark cases for further theoretical and numerical studies.

Large Metro Tunnel Deformation Due to Nearby Excavations: A Case in Eastern China Soft Ground

Engineering Background

This section will discuss a case where a section of the shield metro tunnel was seriously disturbed by large deep excavations nearby. The disrupted part of the tunnel is located in the soft soil area in a recently re-developed city area in Nanjing, China. Excavations caused excessive cross-sectional deformation of the tunnel, and consequently, active mitigating methods were adopted, and in particular, a grouting technique was employed to retrofit the tunnel lining structures.

The twin tunnels under consideration were placed into operation in the year 2010. After two years of service, massive excavations took place in the close vicinity of the tunnels on both sides as part of the construction for the substructure of ten high-rise towers (office buildings of 120 m to 200 m in height) in the city's financial center. The entire excavation site was split into four major zones, where Zone I and Zone III, being the ones adjacent to the tunnels, were recognized to be the primary reason for the over-deformation of the tunnels. Therefore, this paper will focus the attention on these two zones.

The geology of this area is distinguished by a typical layer-structured soft deposit of the Yangtze river delta. The stratum comprises primarily of the made-ground, muddy silty clay, and fine sand. A thick layer of muddy silty clay comprises a significant proportion of the upper stratum, which is high in water content (around 40 %), low in strength (the undrained shear strength commonly below 35kPa) and permeability (in the order of 10^{-6}-10^{-5} mm/s), and high in compressibility (the compression coefficient $\alpha_{0.1-0.2}$ ranges between 0.6 and 0.8 MPa^{-1}). These characteristic values are comparable with that of the soft deposits in Shanghai (Zhang, et al., 2018), and thus the soil shares similar engineering properties. Engineering experience suggests that these soils tend to decrease significantly in strength once disturbed, resulting in prolonged deformational behaviors (Tan and Li, 2011, Tan and Wei, 2012, Yin and Chang, 2009). Under the muddy silty clay, the fine sand constitutes another major thick layer with much higher permeability (in the order of 10^{-2} mm/s). Beneath the fine sand layer, layers of coarse sand and weathered mudstone find their places. Fig. 1 demonstrates the spatial relationship between the two tunnels and Zone I and Zone III of the excavation. Fig. 1(b) presents the representative geological profile at the construction site corresponding to the cross-section of A-A, which is derived from the borehole results. At the grouting test region, the soil layer thicknesses of the made-ground and the muddy silty clay were estimated to be around 4.7 to 5.7 m, and 24 to 26 m, respectively. Detailed soil parameters are summarized in Table 1.

Fig. 2 displays the design of the segmental tunnel lining. The lining ring is staggered-assembled by six pre-fabricated RC segments, measured 6.2 m in outer diameter, 1.2 m in width, and 0.35 m in thickness. The neighboring pieces are jointed using 400 MPa curved steel bolts both in the longitudinal and circumferential directions.

(Table 1)

(Fig.1)

(Fig.2)

Adjacent Excavations and Rehabilitation of the Over-deformed Tunnel

The excavation activities of Zone I were started in February 2012 and completed in July 2013, marked by the bottom concrete slab casting. In November 2013, the construction of the entire substructure of Zone I came to an end. Shortly after completing the bottom slab casting in Zone I, excavation in Zone III continued to proceed from July 2013. By October 2013, the impact of the excavations became identifiably evident from the pronounced cross-sectional response of the tunnel in terms of considerable convergence.

The deep excavations strongly influenced approximately 300 rings (ring 460 to 760) in the left-line tunnel, with a horizontal convergence ratio ($\Delta D/D$) greater than 0.5 percent, where D is the initial outer diameter of the tunnel (Fig.3). As illustrated in Fig. 4 (a), the tunnel sections under the most severe impact, namely ring 508 to 666 corresponding to Zone I, exhibited a $\Delta D/D$ ratio ranging from 1.02 percent to 1.40 percent, well above the relevant design regulations of 0.3 to 0.5 percent as the serviceability limit for a shield tunnel under normal operating condition (Committee, 2007, GB50157, 2013, Society, 2004).

To maintain the metro line's operational safety, the metro company determined to tackle this problem by adopting grouting procedures at both sides of the over-deformed tunnel to correct the tunnel deformation back to an acceptable level and increase ground resistance. However, the engineering knowledge was quite restricted at that time regarding the grouting treatment's achievable effect in reducing the excessive tunnel deformation and the refinement of grouting parameters for the region's particular geological condition. Moreover, understanding the tunnel's detailed spatial and temporal response under the grouting impact was of particular interest, which was rarely reported in the existing literature. In view of these, a field grouting test on a particular section of the left-line tunnel (ring 580 to 588) was performed before the full-scale implementation of the technique.

The experiment was performed between Oct 30, 2013, and Nov 10, 2013. It should be mentioned that as the grouting tests were performed, excavation in Zone I had already been completed, and excavation in Zone III was constructed at its third level. Due to the long distance between the excavation pit to the testing tunnel, the excavation-induced effect on the tunnel was anticipated to be negligible in the short term. Therefore, the grouting effects were considered the governing factor of the tunnel's deformational response.

Grouting Experiment

Grouting Procedures

Fig. 3 illustrates the composition of the grouting system. The general idea was to extend grouting conductors from the ground surface to the designated grouting position in the vicinity of the tunnel to achieve grout injection. Before the grouting procedures, the tunnel's exact position was measured in terms of its burial depth and the exterior surface (extrados) coordinates. Afterward, holes were drilled from the ground to the bottom level of the tunnel lining extrados (hereafter referred to as the tunnel invert). Casing pipes of similar diameter with the drilled holes were subsequently placed in position inside the holes to prevent soil cave-in and facilitate an easier installation of grouting pipes. After this, a grouting pipe was pushed within the casing pipe to the depth where the lower end of the grouting pipe reached the tunnel's invert elevation. The key components of the grouting system were then assembled to form an effective grouting injection system, which comprises of grouting pumps, flow meter, grouting mixer, and grouting pipes. After successfully installing the grouting injection system, preparation of the cement slurry and sodium silicate was conducted. The grouting operation was carried out utilizing two pumps simultaneously, each responsible for injecting cement (ordinary Portland cement 42.5) and sodium silicate (baume degree (°Be') 35). Initial setting time of the grout slurry affects both the grouting effect and the grouting operability. By changing the mixture ratio of the sodium silicate and Portland cement, the initial setting time of the grouting slurry can be flexibly adjusted. Mixture ratios rendering optimum initial setting time were obtained via a series of laboratory testing, so that plugging of the injection pipe can be avoided and an intended diffusion radius of grout in soil can be reached. The water-cement ratio for the cement slurry was 0.6 to 0.7, and the volume ratio of about (2 to 3):1 was adopted when mixing the cement slurry and sodium silicate. These formulas generated grout slurry with an initial setting time around 10 minutes. Grouting pressure for the site was set around 0.5 MPa, which was constantly monitored by a grouting pressure gauge, and carefully controlled by experienced technicians to avoid pressure anomalies. The grouting flow rate was controlled between 14 to 16 L/min for the cement slurry, and 5 to 10 L/min for the sodium silicate, resulting in a 20 L/min total flow rate. The liquid flow rate was monitored in real-time by a flow meter.

The grouting procedure was established to achieve reduced disruption to the surrounding ground. During the grout injection, the grouting pipe was raised upwards steadily and slowly at a consistent pace by a pipe-lifting system. As such, the uniformity of grout spreading with respect to depth was ensured. At the beginning of the pipe-lifting process, the grouting nozzles at the end of the grouting pipe were automatically exposed to release grout when the front-end hat covering those nozzles was removed (see Fig. 3). The grouting pipe experienced continued lifting until the lower end of the casing pipe. It was kept still for around ten minutes so that the grouting material could experience initial setting. After the setting period, the grouting pipe was raised from the ground by the pipe lifting system to conclude the grouting procedure for one hole.

(Fig.3)

Grouting Testing Arrangements

The grout was injected in a double-row array scheme. The specific dimensions of array positions, named A1, A2, B1, and B2, for installing grouting pipes are illustrated in Fig. 7. The rows were symmetrically positioned with respect to the longitudinal centerline of the left line tunnel, with A2 and B1 positioned nearer to the tunnel.

The grouting zone positions relative to the ground surface can be represented by two individual positioning parameters: the grouting elevation (GE) and the grouting height (GH), as demonstrated in Fig. 7. In this field experiment, various positioning parameters were adopted for different grouting operations to obtain a diverse range of testing cases to observe position-related sensitive effects.

Fig. 7 summarizes the details of the grouting schedules and the corresponding positioning parameters from Oct 30, 2013, to Nov 10, 2013, for tunnel ring 580 to 599. Circles of three distinct colors represent the grouting position to the left line tunnel and the grouting status.

For convenience and simplicity, in this paper, we will name the i^{th} grouting operation in the experiment as stage Gi, and the grouting-free period before the next grouting injection as Ri, instead of referring them by their time of occurrences. We also define the starting time of G1 as time 0, which corresponded to the midnight of Oct 30, 2013 (Fig. 5(a) and Fig.7). In Fig. 7, circles in pink represent inner grout injections at A2 and B1, blue represents outer injections at A1 and B2, and grey circles represent the existing grout injections where consolidation has occurred. Total grouting volumes in liters are also listed for new grout injections of the current grouting operation.

As for the grouting arrangement, the grouting elevations from G1 to G7 (Oct 30 to Nov 6) were 2.7 m higher than the tunnel invert elevation, and the corresponding grouting heights were 5.2 m. However, starting from G8 (Nov 7), the grouting elevation was lowered to match the tunnel invert elevation. Besides, the grouting height was set to 4.2 m in G8 (Nov 7), creating a case with a shorter grouting zone.

Monitoring Scheme

An automatic monitoring scheme was adopted to obtain comprehensive information on the tunnel lining response during the grouting operations. The system comprises a combination of robotic total stations (Type Leica TM30) and reflection prisms, which were mounted to the tunnel lining inner surface at its spring line level (Fig. 2(b)). These monitoring systems can be used to measure the tunnel’s deformational response in both longitudinal and circumferential directions. In this study, the system was mainly used to obtain horizontal convergence of the tunnel for the rings under testing. The accuracy of the aforementioned monitoring system was estimated to be around ± 0.5 mm, based on the calibration tests from similar projects in Nanjing.

The monitoring system allowed the interrogation of the tunnel convergence response in a timely fashion at intended time intervals. During the grouting operations, the time intervals of data acquisition were set to be 5 or 10 minutes, based on the convergence changing rate in the field observation. This time intervals were selected empirically to capture sufficiently detailed tunnel deformational responses during the grouting operations and form coherent deformation curves. During the experiment, real-time monitoring data of the tunnel convergence were obtained and forwarded to the grouting team on the ground surface to facilitate their grouting control judgments. Meanwhile, structural damage in the forms of spalling, cracking, or leakages were also under close inspection by inspectors inside the tunnel during the grouting operations. During the grouting process, alerts were delivered to the grouting team if the convergence reaction surpassed 1.0 mm or minor structural damage was observed during the grouting process. In contrast, the immediate termination of the grouting injection was demanded if a change in convergence exceeded 5.0 mm, or significant structural damage was detected.

Monitoring Results

Overall Deformational Response

The robotic total station began to monitor the convergence evolution of the tunnel on Oct 30, 2013, for the grouting-impacted lining rings (581 to 589). Data were obtained during the grouting-treatment period (Oct 30, 2013, to Nov 10, 2013) and several days after these grouting operations (between Nov 11, 2013, to Dec 7, 2013). The overall change in convergence, relative to the start of the experiment, is shown in Fig. 4(b). It should be mentioned that the convergence time histories presented in Fig. 4(b) are, in fact, the net convergence variation that accumulated between different grouting operations, where the dynamics within a single grouting operation are ignored. It is noticeable that the evolution of the convergence from different rings shares a typical pattern consisting of a recovery stage during the grouting process and a rebound stage following the completion of the grouting treatment. The grouting injections tended to cause the soil's expansion movement around the grouting nozzles during the grouting operations, thus introducing thrust pressure onto the nearby tunnel linings, pushing the rings to retract to a smaller convergence. However, after completing the grouting process, dissipation of positive excess pore pressure and solidification of grout inevitably follows (Soga, et al., 2004). Therefore, the recovered deformation cannot be 100% maintained, and a certain amount of convergence rebound took place.

The convergence recovery and rebound values of all the rings directly under the grouting impact during the entire field experiment are illustrated in Fig. 4(d), where the maximum, minimum, and mean values for each item are also highlighted. Effects of grouting were proved to be remarkable and useful.

Specifically, the average recovered convergence of the rings under testing right after the last grouting operation was reduced by 19.1 mm, about 25% of their average absolute convergence measured before the grouting treatment. Following the completion of the grouting treatment, the rebounding phenomenon led to an increment of the average convergence by 6.5 mm during 20 days. Thus a 12.6 mm average net convergence recovery was measured for the tunnel rings under testing at the termination of the experiment. The convergence rebound may be subjected to the influence of various aspects such as soil permeability and grout properties. An in-depth study of these aspects is beyond the scope of this paper. However, it is worth noting that the ratios of the total rebound values over the recovery values for rings under testing fall into a relatively narrow range, with an average value of 34.3%, as shown in Fig. 4(d). This means, on average, about 65% of the recovered convergence was retained at the completion of the experiment. This observation suggests that the convergence rebound may be estimated in proportion to the convergence recovery response in the engineering practice.

Fig. 4(c) depicts the spatial distribution of the cumulative grout volume injected and the corresponding total convergence recovery response observed at the termination of the selected grouting operations, showing that as more grout was injected and accumulated in the ground, the convergence recovery increased accordingly. It is noticeable that the cumulative grout volume distribution among different rings was substantially uneven for all selected cases. For example, after G11, for the majority of the testing rings, the grout injected was around 3000 liters. However, this amount was doubled for rings 583 and 587. Interestingly, the doubled grouting volume at ring 587 did not seem to result in a greater recovery response as one would normally anticipate. However, a large amount of grout at ring 583 appeared to facilitate the recovery peak formation at ring 584. Similar effects can also be observed for G5 and G7. These observations tend to suggest a less direct correlation between the grouting volume of individual rings and their convergence recovery values. However, the convergence recovery tends to be larger in the grouting zone center (rings 581 to 585) and much smaller around its rim (rings 586 to 589), even if a more considerable amount of grout was injected (for example, in the case of ring 587). Therefore, tunnel convergence response resembled the deflection curve of a beam under distributed pressure, where the most prominent displacement would usually occur around its middle portion, and the details of fluctuations in the pressure distribution would become less critical.

(Fig.4)

Evolution of the Tunnel Lining Response During the Grouting Treatment

While the overall behavior of the tunnel linings during the grouting-treatment stage tends to experience net convergence recovery, as introduced in the previous section, detailed monitoring records with shorter time intervals reveal a dynamical evolution of the convergence accumulating process during the grouting operations.

Fig. 5 demonstrates how the grouting-induced convergence recovery accumulates in time for all rings under testing during the grouting-treatment stage. Fig. 5(b) depicts the evolutional histories of the relative convergence. The values shown are relative convergence comparing to the start of the grouting treatment. It is noticeable that those convergence time histories are featured in similar configurations, taking an upwards zig-zag recovery profiles. The evolutional history curves also suggest that much larger transient tunnel convergence recoveries were achieved within a relatively short period of the grouting operations, which generally only lasted 2 to 3 hours a day around midnight. Afterward, a much longer and slower rebounding phase took over due to the absence of grouting activities, as indicated by the portion of the negative-sloped branches of the convergence recovery curves (Fig. 5(c)). Therefore, the convergence recovery accumulation behaviors in the grouting treatment are observed to resemble the inhale and exhale behavior of a person. This phenomenon is termed the 'breathing effect' in this paper. The net convergence accumulation over one round of grouting operation is the difference between the grouting-induced recovery and the reversal movement in the rebounding phase (Fig. 5(c)).

By separately presenting the effect of grouting and the subsequent rebound for each grouting operation in terms of convergence increments (recovery movement taken as negative), Fig. 5(a) demonstrates the temporal and spatial distribution of the convergence increment for all rings during the grouting treatment, with grouting rings highlighted for clearer observation of the correlation between the grouting location and the tunnel deformation response. The i^{th} grouting stage G_i spans over the initiation and the completion of the i^{th} grouting operation, while the i^{th} rebounding stage R_i starts right after the completion of G_i and terminates at the start of G_{i+1}. In total, 11 of these stage pairs exist according to the field testing record. The incremental convergences at each operational stage in Fig. 5(a) and Fig. 7 are the differential values between the corresponding stage's starting and ending values.

As indicated in Fig. 5(a), it is apparent that the spatial distribution of the grouting-induced convergence response relies on the spatial layout of the grouting injections. Although a clear correlation between the grouting arrangements and the induced tunnel deformational response remains to be further examined, a tendency becomes clear that the rings close to the grouting positions tend to experience a more prominent recovery effect. The columns in Fig. 5(a) that alternate in colors of red and blue indicate the existence of the 'breathing effect'. Meanwhile, the figure also suggests a specific correlation between the recovery and rebound effects of convergence variations: the more significant the convergence recovery, the more likely the tunnel will experience a more considerable subsequent rebound.

To reveal the correlation between the behaviors of convergence recovery and rebound, averaged convergence variation rates (mm/day) are calculated. These data are collectively presented in Fig. 5(f), which illustrates a largely positive correlation between the two variables. Although the data tend to fall into a relative wide band, a linear correlation between the convergence recovery rate and the rebound rate appears to be identifiable up to a certain limit (around 50 mm/day). However, as the convergence recovery grows greater than this limit, the corresponding rebound appears to become stabilized, maintaining at a rate around 0.8 mm/day.

Fig. 5(d) and Fig. 5(e) display selected grouting operations for exemplifying the correlation of the convergence recovery rate and the rebound rate of all rings. As shown in Fig. 5(d), in the 2nd routing operation, the convergence recovery rate and subsequent rebound rate demonstrate relatively consistent distribution profiles over the testing rings. The phenomenon seems reasonable in that the tunnel experienced a relatively small magnitude of the convergence recovery rates during this grouting operation (over a range of 11.2 mm/day to 32.0 mm/day), and all data fall into the linear region categorized in Fig. 5(f). In the case of the 8th grouting operation, the rate of grouting-induced convergence recovery spanned a much broader range from 3.2 mm/day to 89.6 mm/day. The convergence recovery rate profile and the corresponding rebound rate experience a particular difficulty in matching each other. In Fig. 5(e), a close match is attained for the two variables' profiles between the rings 586 to 589, where the convergence recovery rates are relatively low. However, for rings experiencing larger convergence recovery rates, the rebound rate tends to be more stagnant, therefore featuring a departure of the twin curves. This observation also complies with the conclusion drawn from the overall data distribution in Fig. 5(f).

The equation in Fig. 5(f) is arrived to approximate the correlation of the convergence recovery rate and rebound rate when convergence is smaller than 50 mm. The resulting equation could predict the rebounding behavior of the tunnel lining for sites of similar conditions.

(Fig.5)

Tunnel Lining Response During a Single Grouting Operation

A close-up view of the tunnel deformational behaviors during the grouting injection period can be obtained, owing to the availability of the convergence records every 5 to 10 minutes during the grout operations. These observations would be meaningful to understand the evolutional characteristics of the grouting efficiency during a single grouting operation.

Fig. 6 presents the convergence response to the varying grouting injection volume for selected grouting operations. In order to obtain a more precise correlation between the grouting volume and the convergence response, only the single ring grouting results are selected for analysis in this section. Specifically, testing results corresponding to stage G1, G8, and G11 represent single-sided grouting operations, while G3 a double-sided process. These grouting operations adopted varied geometrical arrangements, which are illustrated in detail in Fig. 7.

The grouting volume injected and the corresponding convergence reaction of the tunnel in Fig. 6 have been normalized for a more straightforward comparison between different cases. The normalized grouting volume sequence is the ratio of the grouting volume sequence over the total grouting volume of a particular grouting operation. Similarly, the normalized convergence recovery is obtained by dividing the convergence recovery time history by the maximum measurement value in a specific grouting operation. Despite differences in the grouting geometrical configuration, all convergence responses of the selected cases seem to experience two different stages indicating varied grouting efficiency. Specifically, when the grout injection volume is relatively low, a relatively high grouting efficiency can be attained, featuring a steep slope of the convergence response curve. However, as the grout volume exceeds a specific limit, the effectiveness of the grout injection markedly decreases, and the convergence response curve tends to become increasingly flat. Therefore, a critical grouting volume exists between the high-efficiency grouting stage and the low-efficiency grouting stage, depending on various grouting parameters and geotechnical properties.

Based on the testing results, for the single-sided grouting operations, the critical grouting volume ranges from 300 to 600 liters, while for the double-sided process, this value reaches about 1000 liters. This enhancement is reasonable in that the soil at the other side of the tunnel (opposite to the grouting side) needs to supply enough resistance to facilitate an effective reduction of the convergence. As the double-sided approach can enhance the ground resistance at both sides of the tunnel, the effect translates into the increase of the critical grouting volume, resulting in greater effectiveness in convergence reduction.

(Fig.6)

Spatial Distribution of Grouting-induced Deformational Reaction

As previously mentioned, the grouting effects on the tunnel will gradually diminish with increased grouting distance. However, further understanding of this effect would require information on the specific geometrical details of the grouting operations. Fig. 7 presents the detailed grouting operation history and the corresponding convergence response of the tunnel lining during both the convergence recovering stages and the subsequent rebounding stages. The geometrical arrangement of the grouting operations is elaborated in detail, with the detailed grout injection volumes of each operation displayed.

As illustrated in Fig. 7, grouting operations were conducted to treat single rings, double or triple rings simultaneously during the entire grouting experiment. These arrangements inevitably gave rise to a complex deformational response of the tunnel convergence. The single-ring operations could best serve for observing the spatial distribution of grouting-induced tunnel convergence response. The single ring operations selected as examples for demonstrating the grouting-induced tunnel deformational pattern include grouting operations at one side of the tunnel (G1 and G8) and those conducted at both sides concurrently (as in G3).

These single ring cases actually demonstrate varied deformational patterns. For some cases, a convergence distribution can be clearly identified that resembles the shape of a bell, such as G3 and G8. However, although the most heavily affected rings tend to locate adjacent to the grouting position, they may not necessarily be the ones that are closest to the exact grouting position. One particular example is the case of G11, where the peak of the distribution curve appears to be around 581 to 583, corresponding to the grout injection at 584. In the case of G1, the distribution of the convergence response even featured no apparent bell shape. These phenomena suggest that the attenuation of the grouting effect possesses considerable variability due to the complex migration behavior of the grouting material in the ground. Therefore, the grouting-induced pressure distribution, reflected by the convergence recovery behavior of the tunnel, can be challenging to predict with certainty.

For the multi-ring grouting operations, the superposition of the grouting effect on single rings seems applicable for some cases, such as the case G5 and G7, where the largest convergence recovery occurs right in the middle of the grouted rings. Whereas, for cases such as G9 and G10, direct superposition seems unable to explain the peak location in the grouting-induced convergence distribution.

Apart from the variability arisen from the inherent complexity of the soil medium, another possible reason to affect the structural response of the tunnel could be the distribution of the existing grouting, which could block or alter the migration behaviors of the current grouting. One such example can be demonstrated in G9, where the inner consolidated grout surrounding ring 580 and 582 may well likely act as a barrier for the current grout injection conducted at ring 581, leading to a smaller convergence recovery response comparing with that induced by the free grouting at ring 585. Likewise, this kind of blocking effect can also be observed for case G6, where the pre-existing grout injections at ring 586 and 587 seemed to block the current grouting at ring 587. This gave rise to a much smaller convergence response in comparison with ring 581 and 583.

The existing grouting may also lead to the redirection of the current grouting flow, as can be observed from the tunnel convergence distribution configurations, such as in the cases of G8 and G11. In G8, the existing grouting injections at ring 583 and 584 tended to steer the current grouting pressure to focus on ring 581 rather than the current grouting ring 582. Similarly, in G11, the existing grouting may be the main reason to cause the peak of the convergence profile to shift from the grouting ring 584. This kind of deviation seemed more likely to occur as more grouting accumulated in the ground. The effect on the tunnel response became more complicated to predict than a ground condition with fewer existing grout injections. One such example can be illustrated by G10, where the convergence response of ring 582 was unexpectedly smaller than that of ring 585.

(Fig.7)

Grouting Efficiency and Influencing Factors

The field data suggests that the grouting efficiency in terms of convergence reduction would vary with different grouting parameters, including the grouting history and various geometrical settings.

In section 2.4.3, we introduced the evolution of the grouting efficiency during single grouting operations, where a consistent pattern of the grouting efficiency evolvement has been revealed. In the whole course of the grouting project, the grouting efficiency also seems to experience different stages that vary with time and grouting history.

The experimental dataset tends to suggest an increasing grouting efficiency as more grouts were injected into the ground. These can be demonstrated by observing the convergence response from G1 to G7 when the individual grouting parameters, namely the grouting elevation and grouting height, remained constant (see Fig. 7). As can be seen, when a relatively small amount of grouting injections were carried out, the convergence recovery per grouting volume is relatively low. We hereby adopt a simplified grouting efficiency indicator to quantify the grouting efficiency, which equals the largest convergence recovery over the total grouting volume in the corresponding grouting operations. This value is calculated to range from 0.5mm/ 1000 L to 0.7mm/ 1000 L for operations G1 to G4. Thereafter, for operations G5 to G7, as the grout was injected continuously into the ground to reach a certain level of grouting spatial density, the efficiency of grouting start to see a substantial increase, as the grouting efficiency indicator raises to the range of 1.0 mm/1000 L to 1.5 mm/1000 L. This phenomenon may be related to the modified soil properties due to the penetration and consolidation of the existing grouting. The details of related mechanisms are subject to further research beyond the scope of the current paper.

Another aspect that is deemed to contribute to determining the grouting efficiency is the geometrical arrangement of the grouting operations. One particular example can be seen from case G8, which was associated with a shorter grouting height (4.2 m) than the other cases (5.2 m). This grouting arrangement resulted in a marked effect on the tunnel deformational response, with the grouting efficiency indicator increased up to 4.6 mm/1000 L. Due to this shortened grouting height, the grouting zone at G8 tended to be more localized, leading to a more concentrated pressure distribution to the adjacent tunnel linings, and this was also clearly reflected by the fast-diminishing bell-shape configuration of the convergence distribution as distance increased. The grouting setting of G8, though exhibiting high grouting efficiency, may also accompany high structural safety risks due to intensified pressure localization, thus should be judged with care in grouting practice.

The grouting elevation effect can be analyzed by comparing cases G5 to G7 with G9 to G11, as they share the same grouting height but different grouting elevations. Meanwhile, they belong to a similar grouting stage, having surpassed the early low-efficiency stage. The grouting efficiency indicator for G5, G6, and G7 is calculated to be 1.47 mm/ 1000 L, 1.04 mm/1000 L, and 1.02 mm/1000 L. The corresponding values for G9, G10, and G11 are 1.28, 1.22, and 1.45, respectively. These results suggest that a lowered grouting elevation tends to yield a slightly higher grouting efficiency in terms of the tunnel deformational response.

A more detailed analysis of the geometrical factors over the efficiency of the grouting operations would require appropriate numerical and theoretical analyses, as the influences of the individual grouting parameters are difficult to decouple based on the field testing dataset alone. These analyses will be presented separately as our continued research.

The Convergence Rebounding after Grouting Treatment

As introduced in the previous sections, the tunnel lining convergence rebound occurred right after completing the grouting operations. The rebounding movements of the lining rings were constantly interrupted by the subsequent grouting-induced convergence recoveries during the grouting treatment period. However, after completing all the grouting operations (starting from stage R11), the continued recording of the tunnel deformation provided an opportunity to observe the undisturbed rebounding performance of the tunnel lining response.

Fig. 8(a) depicts the rebounded convergence evolution for all rings under testing right after the completion of all grouting operations. Overall, these curves demonstrate a similar evolvement pattern where the convergence rebound tends to experience faster incremental rates at the early phase of the rebound, followed by a gradually decaying rate over time. The spatial and temporal distribution of the daily-averaged convergence rebounding rate is calculated and summarized in Fig. 8(b) based on the convergence data. Interestingly, the convergence rebounding rate of all rings only peaked at time 2.0 to 2.5 days after completing the grouting treatment (peaking at 0.8 mm/day), before the decaying process.

Before the peak value, the lining rings experienced a lower rebounding rate right after all grouting treatment.

The time history of the convergence rebounding rate after G11 for rings 583 to 585 is presented in Fig. 8(c), corresponding to the last grouting operation conducted at ring 584. Recordings of other rings are found to share a similar evolvement pattern. It is noticeable that the initial rebounding rate, measured by the convergence change over the first 24 hours after grouting, was only about 0.3 mm/day. This value experienced a speed-up on day two to reach about 0.7 mm/day. After this, it started to decrease. Although the convergence rate peaks vary in magnitudes among rings 583 to 585, a remarkably consistent evolutional pattern can be uncovered of the convergence response during the post-grouting-treatment period when normalization was applied to the data using the respective peak values. Fig. 8(d) demonstrates the evolution of the normalized convergence rate of these rings during the post-peak period. An exponential curve is found to fit the data best and adequately characterize the decaying process. A nonlinear curve fitting program is introduced to obtain the fitted equation employing the Marquardt-Levenburg algorithm (Press, et al., 1992). The relevant statistic parameters are also illustrated in the figure. The fit curve may be expressed by the following formula:

$$y = e^{-0.13682t} \tag{1}$$

The above decay formula may be used for the prediction of tunnel lining responses in grouting projects carried out in muddy silty clay having a similar geological history. It is noticeable that the rebounding rate did not reduce to zero within the observed period. However, using the decay curve in Eq. 1, an estimate of the duration for a given convergence rebounding level can be easily obtained. For example, in the current case, it would take 17 days for 90% of the rebounding rate to disappear.

(Fig.8)

Summary and Conclusions

A large-scale field experiment has been conducted to investigate the effects of grouting treatment on the convergence recovery of the lining structures for an operational shield metro tunnel in Eastern China soft ground. Thanks to the comprehensive monitoring records, the real performance of the tunnel lining has been evaluated both during and after the grouting treatment period. The grouting-induced tunnel response is examined in multiple temporal resolution levels, and this has been made possible by the short measurement intervals (5 to 10 minutes) of the monitoring data. During the experiment, varied geometrical grouting parameters were adopted, enabling a comparison of the effects of different spatial factors. Key findings from the experiment can be summarized below.

(a) The grouting treatment was proved effective in terms of rehabilitating the over deformed tunnel. During the overall course of the grouting experiment, two phases of the tunnel lining deformational response were observed, namely a convergence recovery during the grouting treatment and a convergence rebound after the termination of the grouting treatment. On average, about 25% of the absolute convergence was recovered during the grouting treatment period, and 65% of the recovered convergence was retained after the convergence rebounding stage. Data analysis also reveals that the rebounded convergence tends to be proportional to the recovered convergence, with an average value of 35 % approximately.

(b) Detailed monitoring records with shorter time intervals reveal a dynamic evolution of the convergence accumulating process during the grouting operations. In a single grouting operation, the tunnel convergence is observed to experience a swift recovery followed by a much slower rebound. The accumulation of the convergence recovery over time resembles an upward zig-zag pattern. Further data analysis suggests that the recovery and rebound movements tend to be linearly correlated up to a certain threshold. After surpassing this threshold, the nonlinear response starts to kick in.

(c) The grouting efficiency tends to evolve with time, both for the single grouting operations and for the entire process of the grouting treatment. For single grouting operations, grouting tends to be more effective at the early phase of injections and becomes less effective as a specific grouting volume limit is exceeded. This phenomenon would suggest that it is possible to reduce the amount of the grout injected in the engineering practice, thus the associating costs, while still achieving a similar effect in rehabilitating the tunnel by avoiding the injected grouting volume to enter the low-efficiency zone. The opposite trend is observed for the entire process of the grouting treatment, with a relatively low grouting effect at the start of the grouting treatment and higher efficiency as more grouts are injected, most likely owing to the grouting-induced soil modification.

(d) The specific grouting geometrical layout and grouting history tend to play a critical role in determining the grouting-induced convergence recovery profile. A single ring grouting tends to form a convergence distribution that resembles the shape of a bell. However, the actual convergence distribution may be altered by the barrier or redirecting effects due to the presence of existing grout injections. These observed phenomena could be leveraged to achieve a better grouting effect in practice. For example, grouting at the far-side array first before carrying on at the near-side would potentially enhance the grouting effect in reducing tunnel convergence.

(e) The testing data suggests that for the undisturbed convergence rebound, the convergence rebounding rate only peaked at 2.0 to 2.5 days after the termination of grouting treatment, and the rate over the first 24 hours after the grouting completion was relatively lower. After the peak, the convergence rebounding rate tended to decay exponentially. The test revealed that it would take 17 days for 90% of the rebounding rate to disappear for tunnels buried in muddy silty clay.

Overall, this paper presents a comprehensive case study with new insights into the grouting-induced effects on the temporal and spatial responses of the tunnel lining rings. The detailed information, analysis, and suggestions from this study could serve as a reference for similar grouting projects conducted in the geological context of muddy silty clay. Moreover, the case study also forms a benchmark for further theoretical and numerical studies. It should be noted that some of the characteristics observed would require further research to understand and quantify better.

Data Availability Statement

All data, models, and code generated or used during the study appear in the submitted article.

Acknowledgements

The authors would like to acknowledge the financial support provided by the National Key Research and Development Program of China (2020YFC1511900) and the Fundamental Research Funds for the Central Universities (2242021k30010). The first author would also like to thank Prof. Yuchuan Tang in Southeast University for his valuable comments and suggestions for the paper.

References

Ai, Q., Yuan, Y., Mahadevan, S., and Jiang, X. (2017). "Maintenance strategies optimisation of metro tunnels in soft soil." *Structure and Infrastructure Engineering*, 13(8), 1093-1103. https://doi.org/10.1080/15732479.2016.1243564

Burford, D. (1988). "Heave of tunnels beneath the Shell Centre, London, 1959–1986." *Geotechnique*, 38(1), 135-137. https://doi.org/10.1680/geot.1988.38.1.135

Chang, C.-T., Sun, C.-W., Duann, S., and Hwang, R. N. (2001). "Response of a Taipei Rapid Transit System (TRTS) tunnel to adjacent excavation." *Tunnelling and Underground Space Technology*, 16(3), 151-158. https://doi.org/10.1016/s0886-7798(01)00049-9

Chang, C.-T., Wang, M.-J., Chang, C.-T., and Sun, C.-W. (2001). "Repair of displaced shield tunnel of the Taipei rapid transit system." *Tunnelling and Underground Space Technology*, 16(3), 167-173. https://doi.org/10.1016/s0886-7798(01)00050-5

Chen, R., Meng, F., Li, Z., Ye, Y., and Ye, J. (2016). "Investigation of response of metro tunnels due to adjacent large excavation and protective measures in soft soils." *Tunnelling and Underground Space Technology*, 58, 224-235. https://doi.org/10.1016/j.tust.2016.06.002

Cheng, W.-C., Song, Z.-P., Tian, W., and Wang, Z.-F. (2018). "Shield tunnel uplift and deformation characterisation: A case study from Zhengzhou metro." *Tunnelling and Underground Space Technology*, 79, 83-95. https://doi.org/10.1016/j.tust.2018.05.002

Committee, T. E. (2007). "Standard specifications for tunneling-2006: Shield tunnels." *Jpn. Soc. Civil Eng.*

Cooper, M., Chapman, D., Rogers, C., and Chan, A. (2002). "Movements in the Piccadilly Line tunnels due to the Heathrow Express construction." *Géotechnique*, 52(4), 243-257. https://doi.org/10.1680/geot.2002.52.4.243

Farrell, R. P. (2015). "Tunnelling and compensation grouting at Bond Street, London." *Proceedings of the Institution of Civil Engineers-Geotechnical Engineering*, 168(6), 471-482. https://doi.org/10.1680/jgeen.14.00162

GB50157, M. (2013). "Code for design of metro." Ministry of Housing and Urban-Rural Development of the People’s Republic of China

Han, T., Zhao, J., and Li, W. (2020). "Smart-Guided Pedestrian Emergency Evacuation in Slender-Shape Infrastructure with Digital Twin Simulations." *Sustainability*, 12(22), 9701. https://doi.org/10.3390/su12229701

Huang, H.-w., and Zhang, D.-m. (2016). "Resilience analysis of shield tunnel lining under extreme surcharge: Characterization and field application." *Tunnelling and Underground Space Technology*, 51, 301-312. https://doi.org/10.1016/j.tust.2015.10.044

Huang, H., Shao, H., Zhang, D., and Wang, F. (2017). "Deformational responses of operated shield tunnel to extreme surcharge: a case study." *Structure and Infrastructure Engineering*, 13(3), 345-360. https://doi.org/10.1080/15732479.2016.1170156

Huang, X., Schweiger, H. F., and Huang, H. (2013). "Influence of deep excavations on nearby existing tunnels." *International Journal of Geomechanics*, 13(2), 170-180. https://doi.org/10.1061/(asce)gm.1943-5622.0000188

Jin, D., Yuan, D., Li, X., and Zheng, H. (2018). "An in-tunnel grouting protection method for excavating twin tunnels beneath an existing tunnel." *Tunnelling and Underground Space Technology*, 71, 27-35. https://doi.org/10.1016/j.tust.2017.08.002

Kiriyama, K., Kakizaki, M., Takabayashi, T., Hirosawa, N., Takeuchi, T., Hajohta, H., Yano, Y., and Imafuku, K. (2005). "Structure and construction examples of tunnel reinforcement method using thin steel panels." *Nippon Steel Technical Report*, 92, 45-50.

Komiya, K., Soga, K., Akagi, H., Jafari, M., and Bolton, M. (2001). "Soil consolidation associated with grouting during shield tunnelling in soft clayey ground." *Geotechnique*, 51(10), 835-846. https://doi.org/10.1680/geot.2001.51.10.835

Lee, S.-W. (2002). "The use of compensation grouting in tunnelling: a case study." *Proceedings of the Institution of Civil Engineers-Geotechnical Engineering*, 155(2), 101-109. https://doi.org/10.1680/geng.155.2.101.38653

Li, M.-G., Wang, J.-H., Chen, J.-J., and Zhang, Z.-J. (2017). "Responses of a newly built metro line connected to deep excavations in soft clay." *Journal of Performance of Constructed Facilities*, 31(6), 04017096. https://doi.org/10.1061/(asce)cf.1943-5509.0001091

Li, X., and Chen, X. (2012). "Using grouting of shield tunneling to reduce settlements of overlying tunnels: case study in Shenzhen metro construction." *Journal of construction engineering and management*, 138(4), 574-584. https://doi.org/10.1061/(asce)co.1943-7862.0000455

Li, X., and Yuan, D. (2016). "Development of the safety control framework for shield tunneling in close proximity to the operational subway tunnels: case studies in mainland China." *SpringerPlus*, 5(1), 527. https://doi.org/10.1186/s40064-016-2168-7

Liu, G.-B., Huang, P., Shi, J.-W., and Ng, C. W. W. (2016). "Performance of a deep excavation and its effect on adjacent tunnels in Shanghai soft clay." *Journal of Performance of Constructed Facilities*, 30(6), 04016041. https://doi.org/10.1061/(asce)cf.1943-5509.0000891

Liu, X., Bai, Y., Yuan, Y., and Mang, H. A. (2016). "Experimental investigation of the ultimate bearing capacity of continuously jointed segmental tunnel linings." *Structure and Infrastructure Engineering*, 12(10), 1364-1379. https://doi.org/10.1080/15732479.2015.1117115

Mair, R. (2008). "Tunnelling and geotechnics: new horizons." *Géotechnique*, 58(9), 695-736. https://doi.org/10.1680/geot.2008.58.9.695

Mohamad, H., Soga, K., Bennett, P. J., Mair, R. J., and Lim, C. S. (2012). "Monitoring Twin Tunnel Interaction Using Distributed Optical Fiber Strain Measurements." *Journal of Geotechnical and Geoenvironmental Engineering*, 138(8), 957-967. https://doi.org/10.1061/(asce)gt.1943-5606.0000656

Pinto, F., and Whittle, A. J. (2014). "Ground movements due to shallow tunnels in soft ground. I: analytical solutions." *Journal of geotechnical and geoenvironmental engineering*, 140(4), 04013040. https://doi.org/10.1061/(asce)gt.1943-5606.0000948

Press, W. H., Teukolsky, S. A., Flannery, B. P., and Vetterling, W. T. (1992). *Numerical recipes in Fortran 77: volume 1, volume 1 of Fortran numerical recipes: the art of scientific computing*, Cambridge university press.

Shen, S.-L., Wu, H.-N., Cui, Y.-J., and Yin, Z.-Y. (2014). "Long-term settlement behaviour of metro tunnels in the soft deposits of Shanghai." *Tunnelling and Underground Space Technology*, 40, 309-323. https://doi.org/10.1016/j.tust.2013.10.013

Shi, P., and Li, P. (2015). "Mechanism of soft ground tunnel defect generation and functional degradation." *Tunnelling and Underground Space Technology*, 50, 334-344. https://doi.org/10.1016/j.tust.2015.08.002

Society, B. T. (2004). *Tunnel lining design guide*, Thomas Telford.

Soga, K., Au, S., Jafari, M., and Bolton, M. (2004). "Laboratory investigation of multiple grout injections into clay." *Geotechnique*, 54(2), 81-90. https://doi.org/10.1680/geot.54.2.81.36333

Tan, Y., and Li, M. (2011). "Measured performance of a 26 m deep top-down excavation in downtown Shanghai." *Canadian Geotechnical Journal*, 48(5), 704-719. https://doi.org/10.1139/t10-100

Tan, Y., Li, X., Kang, Z., Liu, J., and Zhu, Y. (2015). "Zoned excavation of an oversized pit close to an existing metro line in stiff clay: Case study." *Journal of Performance of Constructed Facilities*, 29(6), 04014158. https://doi.org/10.1061/(asce)cf.1943-5509.0000652

Tan, Y., and Wei, B. (2012). "Observed behaviors of a long and deep excavation constructed by cut-and-cover technique in Shanghai soft clay." *Journal of Geotechnical and Geoenvironmental Engineering*, 138(1), 69-88. https://doi.org/10.1061/(asce)gt.1943-5606.0000553

Yin, Z.-Y., and Chang, C. S. (2009). "Microstructural modelling of stress-dependent behaviour of clay." *International Journal of Solids and Structures*, 46(6), 1373-1388. https://doi.org/10.1016/j.ijsolstr.2008.11.006

Zhang, D.-M., Huang, Z.-K., Wang, R.-L., Yan, J.-Y., and Zhang, J. (2018). "Grouting-based treatment of tunnel settlement: Practice in Shanghai." *Tunnelling and Underground Space Technology*, 80, 181-196. https://doi.org/10.1016/j.tust.2018.06.017

Zhang, D.-m., Liu, Z.-s., Wang, R.-l., and Zhang, D.-m. (2019). "Influence of grouting on rehabilitation of an over-deformed operating shield tunnel lining in soft clay." *Acta Geotechnica*, 14(4), 1227-1247. https://doi.org/10.1007/s11440-018-0696-8

Zhao, H., Liu, X., Bao, Y., Yuan, Y., and Bai, Y. (2016). "Simplified nonlinear simulation of shield tunnel lining reinforced by epoxy bonded steel plates." *Tunnelling and Underground Space Technology*, 51, 362-371. https://doi.org/10.1016/j.tust.2015.10.004

Zheng, G., Pan, J., Cheng, X., Bai, R., Du, Y., Diao, Y., and Ng, C. W. W. (2020). "Use of Grouting to Control Horizontal Tunnel Deformation Induced by Adjacent Excavation." *Journal of Geotechnical and Geoenvironmental Engineering*, 146(7), 05020004. https://doi.org/10.1061/(asce)gt.1943-5606.0002276

Zhi-jun, D. (2011). "Experimental study of two-shot micro-disturbance reinforced grouting." *Chinese Journal of Underground Space and Engineering*, 7, 1344-1346.

Zhou, S., Xiao, J., Di, H., and Zhu, Y. (2018). "Differential settlement remediation for new shield metro tunnel in soft soils using corrective grouting method: case study." *Canadian Geotechnical Journal*, 55(12), 1877-1887. https://doi.org/10.1139/cgj-2019-0045

Zhu, M., Gong, X., Gao, X., Liu, S., and Yan, J. (2019). "Remediation of Damaged Shield Tunnel Using Grouting Technique: Serviceability Improvements and Prevention of Potential Risks." *Journal of Performance of Constructed Facilities*, 33(6), 04019062. https://doi.org/10.1061/(asce)cf.1943-5509.0001335

List of Table

Table 1. Soil parameters.

Soil layer	w	γ	e_o	c	ϕ	I_P	I_L	$Es_{0.1\text{-}0.2}$	N
Muddy silty clay	41.8	17.3	1.210	19	12.3	15.3	1.17	3.03	1.8
Fine sand	26.8	18.2	0.838	10	33.8	-	-	10.58	12.0

w water content (%); γ unit weight (kN/m^3); e_o void ratio; cohesion c (kPa); ϕ fiction angle (°); I_P plastic index (%); I_L liquid index (%); $Es_{0.1\text{-}0.2}$ compressive modulus (MPa); N, corrected SPT N value

List of Figures

Fig.1(a)

Click here to access/download;Figure;Fig.1a.pdf

(a)

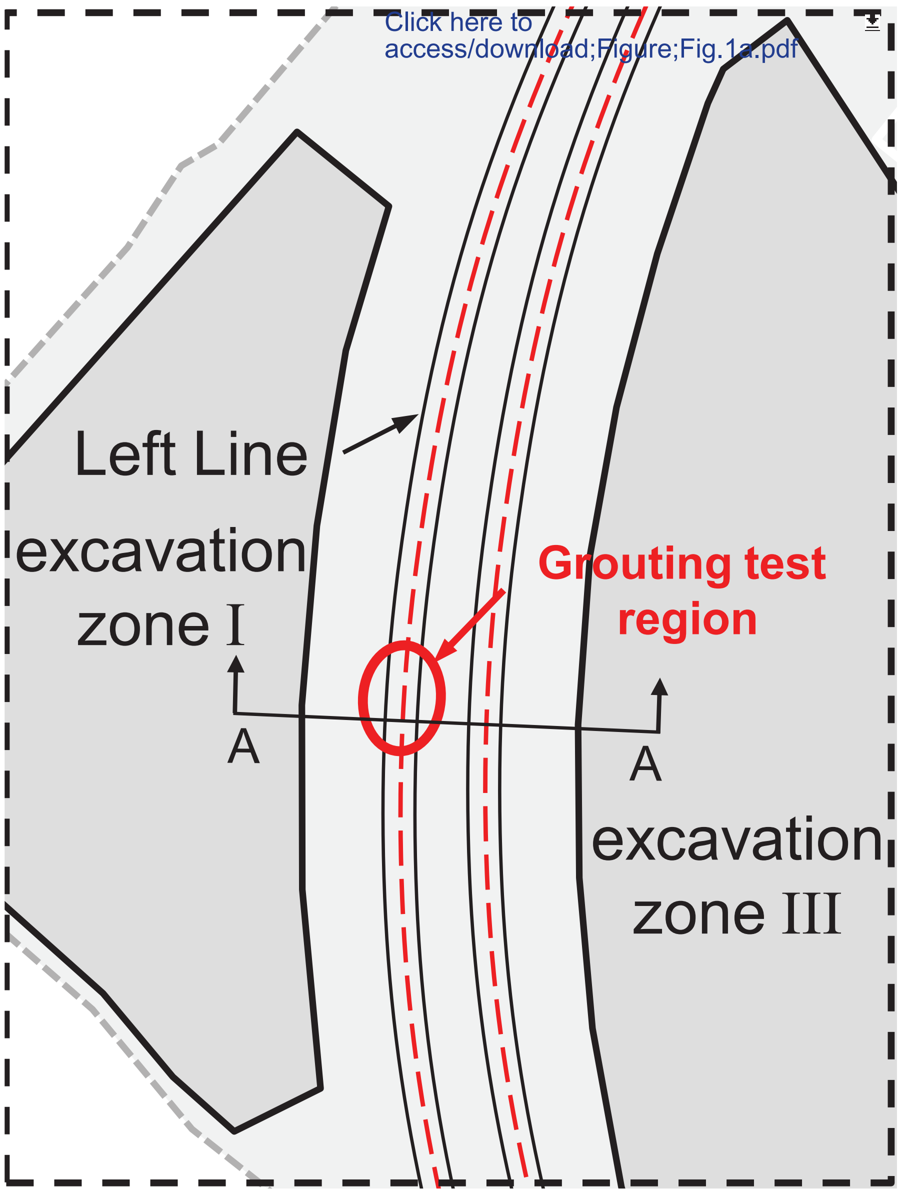

Fig.1(b)

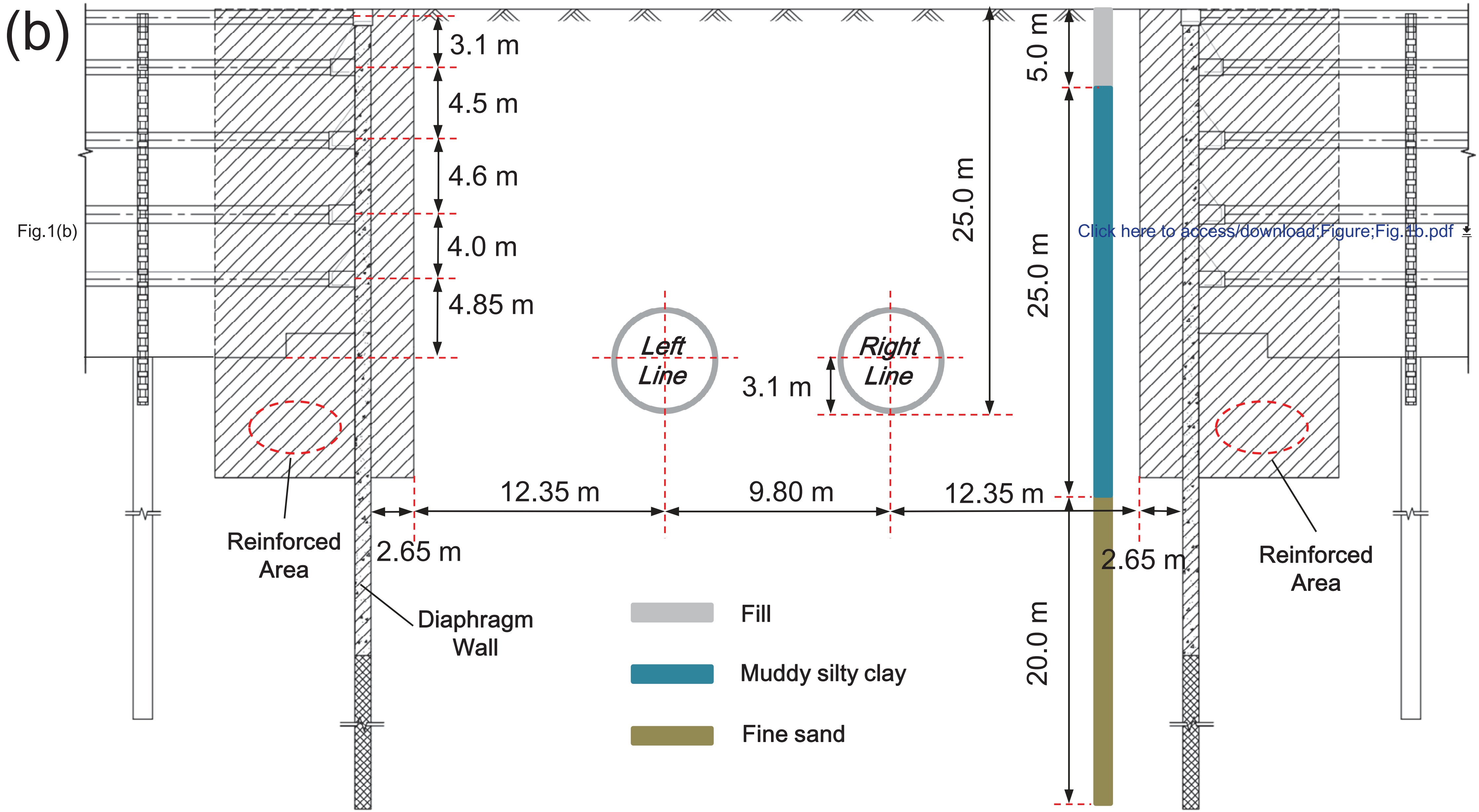
(b)
3.1 m
4.5 m
4.6 m
4.0 m
4.85 m
Left Line
Right Line
3.1 m
25.0 m
5.0 m
25.0 m
20.0 m
12.35 m
9.80 m
12.35 m
2.65 m
2.65 m
Reinforced Area
Reinforced Area
Diaphragm Wall
Fill
Muddy silty clay
Fine sand

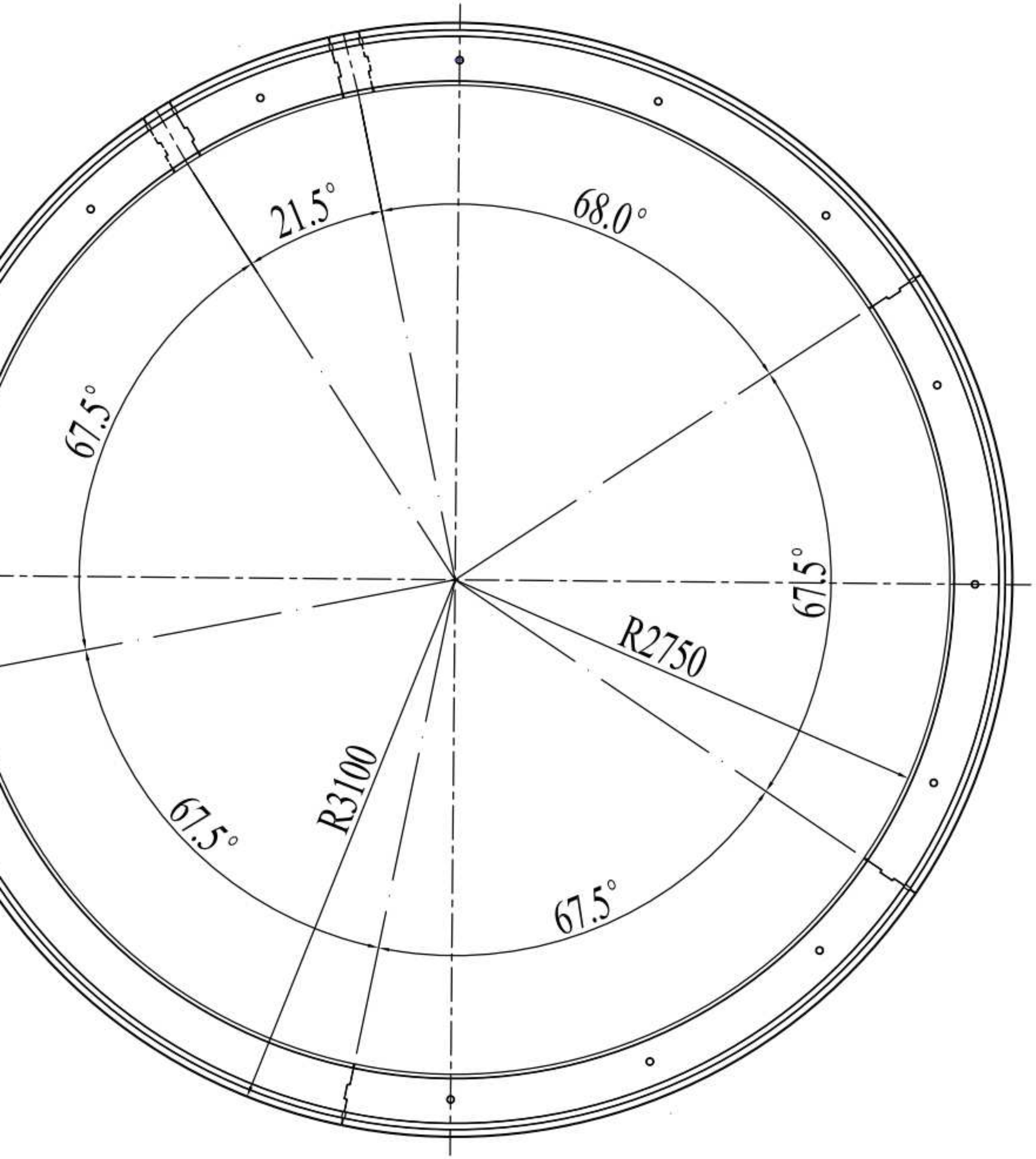
21.5°
68.0°
67.5°
67.5°
R2750
R3100
67.5°
67.5°

(b)

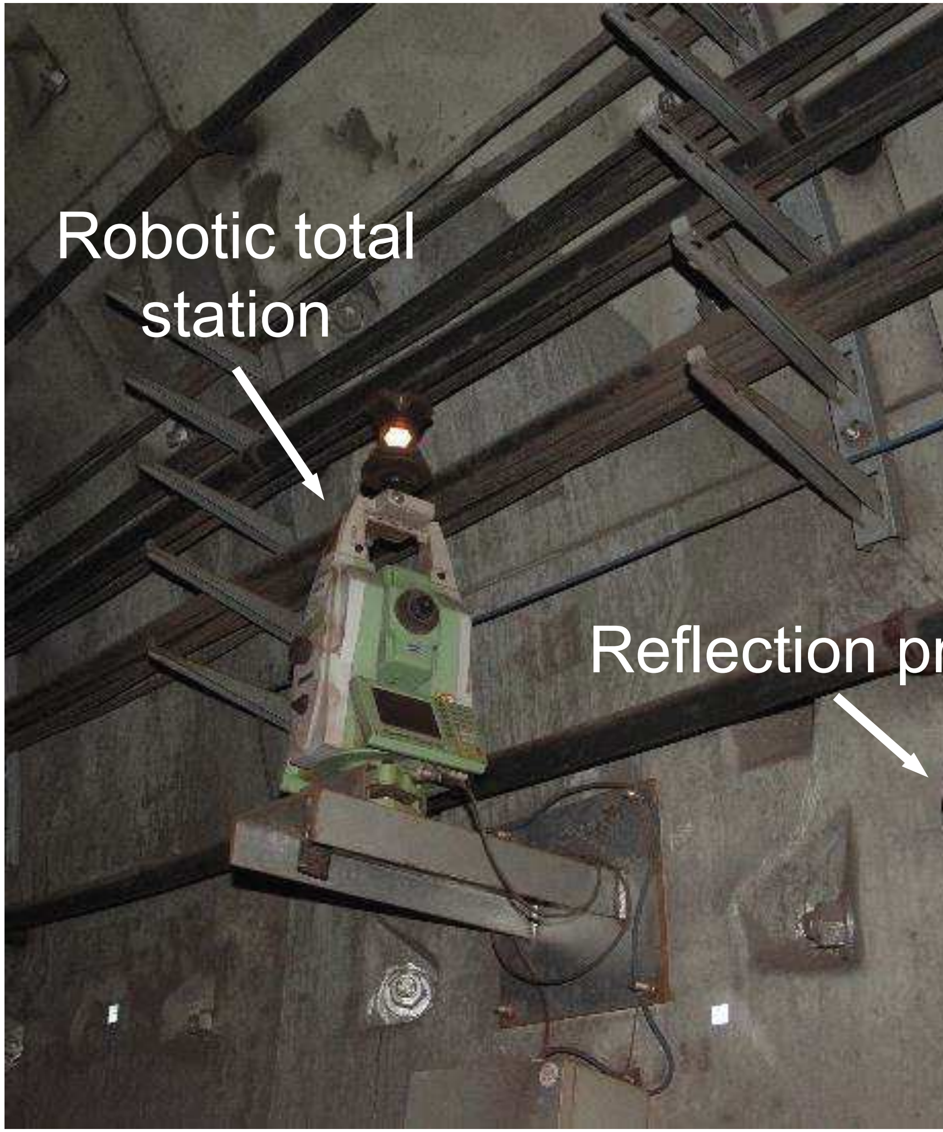
Robotic total station
Reflection pr

updated Fig.3

Click here to access/download;Figure;Fig 3 new.pdf

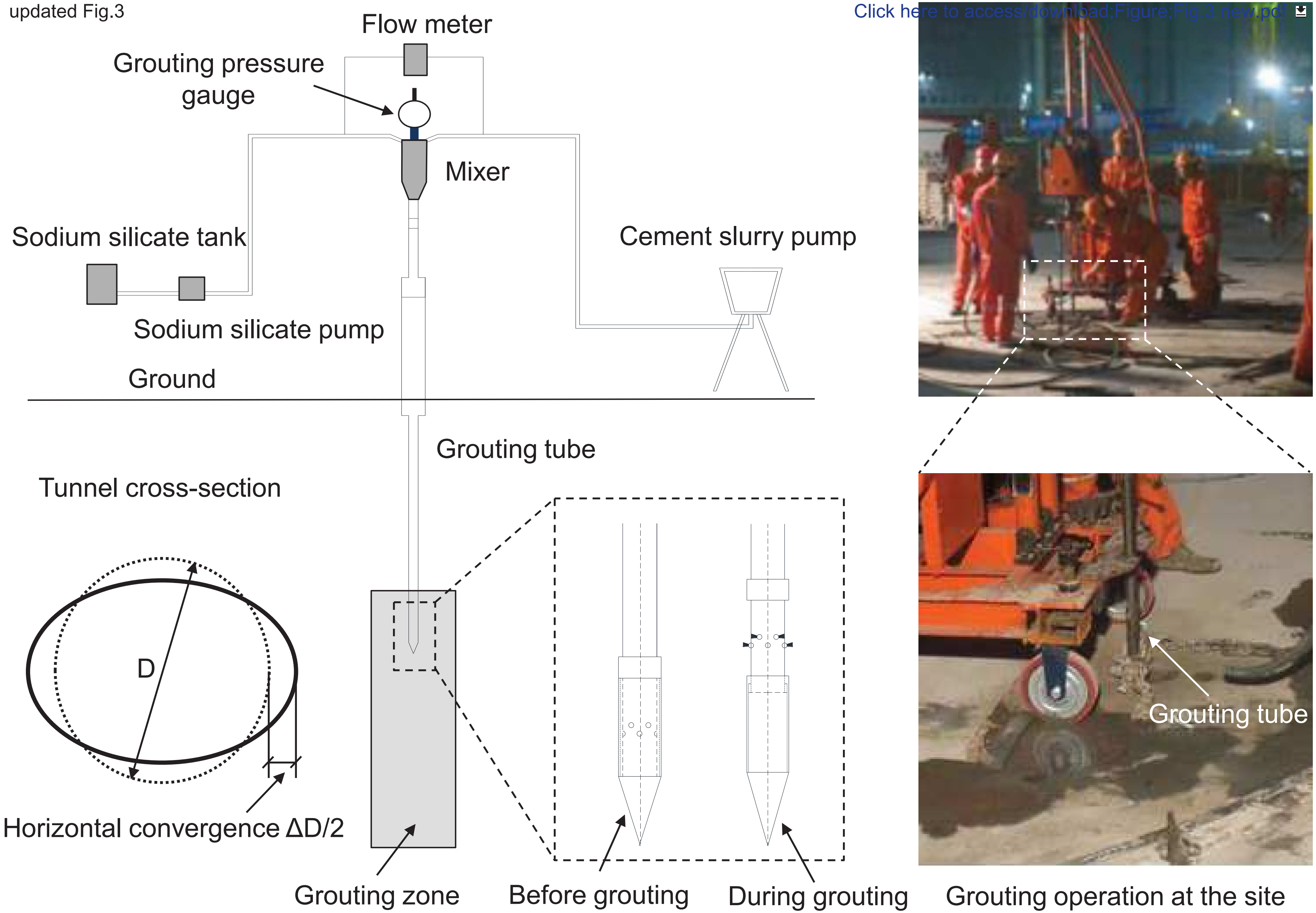

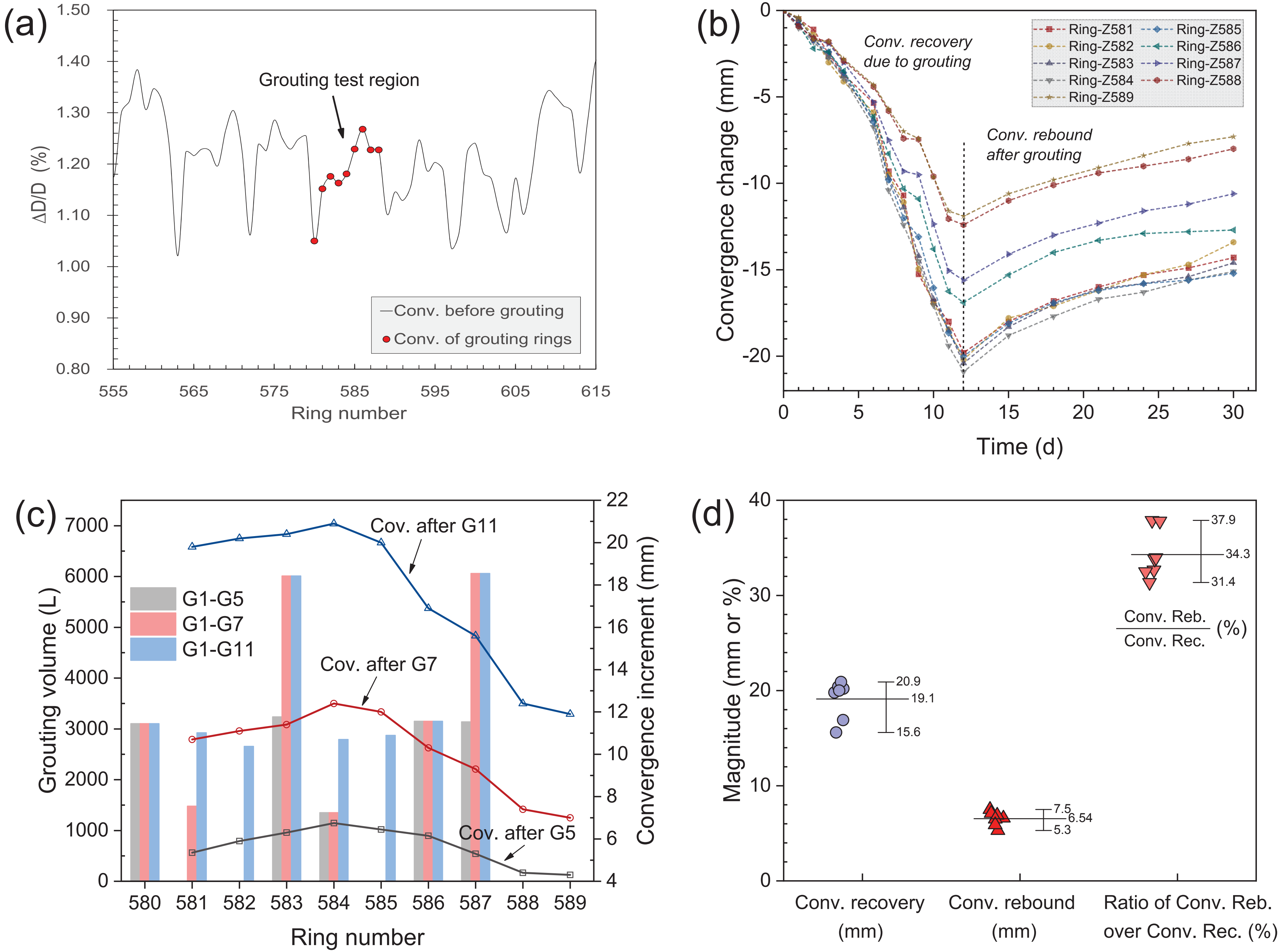

(a)
Grouting test region
ΔD/D (%)
Ring number
Conv. before grouting
Conv. of grouting rings
(b)
Conv. recovery due to grouting
Conv. rebound after grouting
Ring-Z581
Ring-Z582
Ring-Z583
Ring-Z584
Ring-Z585
Ring-Z586
Ring-Z587
Ring-Z588
Ring-Z589
Convergence change (mm)
Time (d)
(c)
G1-G5
G1-G7
G1-G11
Cov. after G11
Cov. after G7
Cov. after G5
Grouting volume (L)
Convergence increment (mm)
Ring number
(d)
Magnitude (mm or %)
Conv. Reb. / Conv. Rec. (%)
37.9
34.3
31.4
20.9
19.1
15.6
7.5
6.54
5.3
Conv. recovery (mm)
Conv. rebound (mm)
Ratio of Conv. Reb. over Conv. Rec. (%)

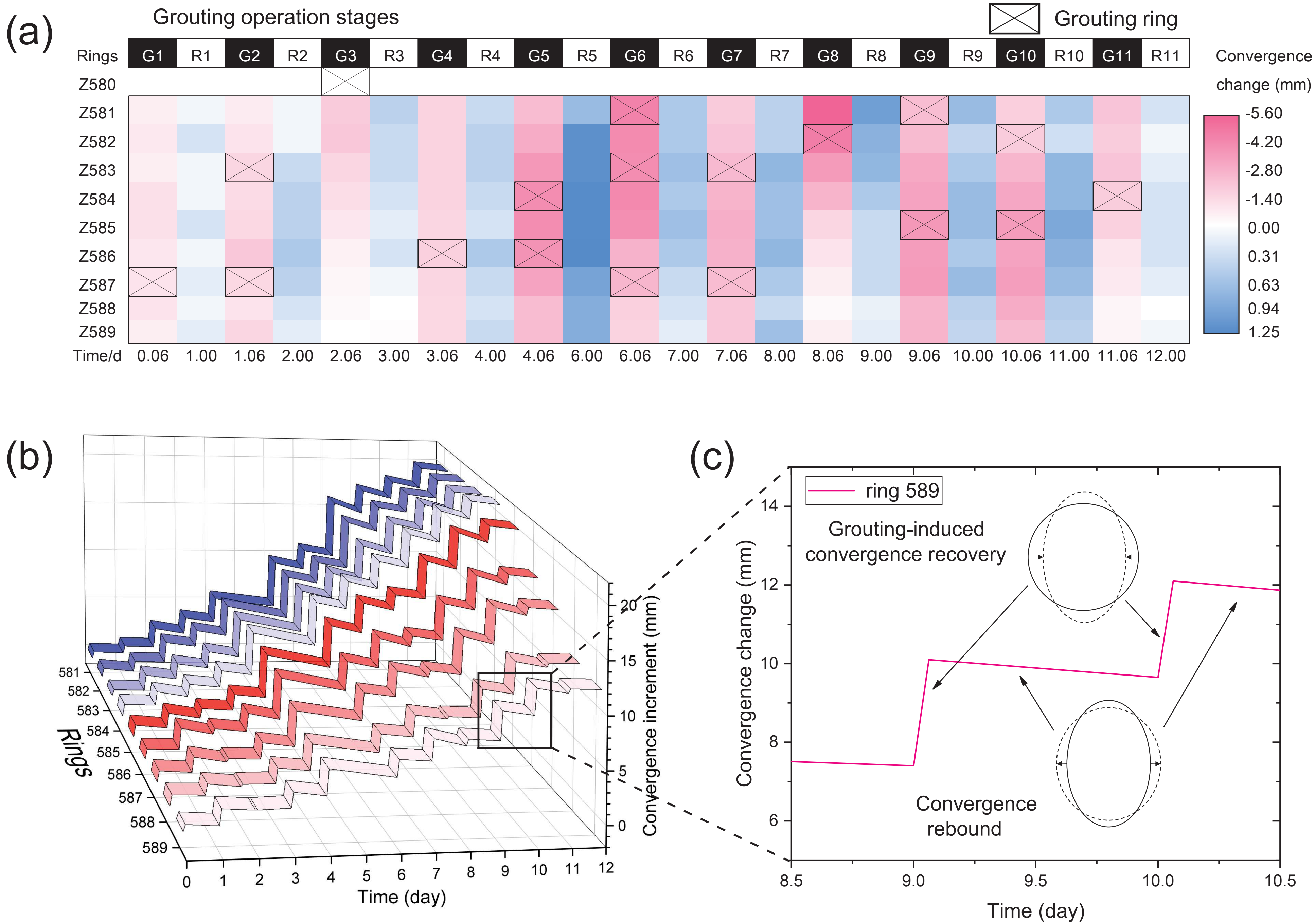

(a)
Grouting operation stages
Grouting ring
Rings
G1 R1 G2 R2 G3 R3 G4 R4 G5 R5 G6 R6 G7 R7 G8 R8 G9 R9 G10 R10 G11 R11
Z580
Z581
Z582
Z583
Z584
Z585
Z586
Z587
Z588
Z589
Time/d
0.06 1.00 1.06 2.00 2.06 3.00 3.06 4.00 4.06 6.00 6.06 7.00 7.06 8.00 8.06 9.00 9.06 10.00 10.06 11.00 11.06 12.00
Convergence change (mm)
-5.60
-4.20
-2.80
-1.40
0.00
0.31
0.63
0.94
1.25
(b)
Rings
Time (day)
Convergence increment (mm)
(c)
ring 589
Grouting-induced convergence recovery
Convergence rebound
Convergence change (mm)
Time (day)

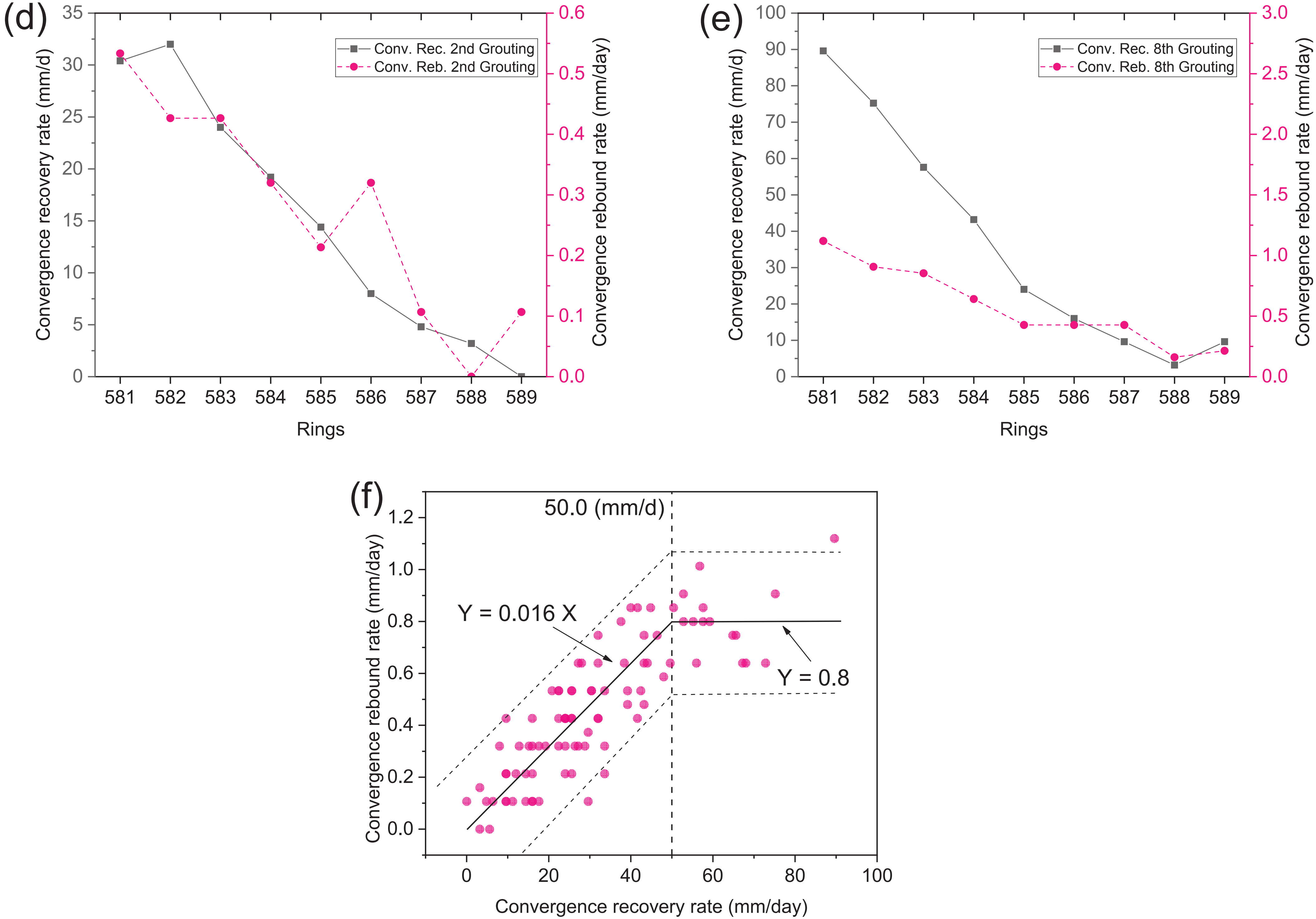
(d)
Convergence recovery rate (mm/d)
Convergence rebound rate (mm/day)
Conv. Rec. 2nd Grouting
Conv. Reb. 2nd Grouting
Rings
(e)
Convergence recovery rate (mm/d)
Convergence rebound rate (mm/day)
Conv. Rec. 8th Grouting
Conv. Reb. 8th Grouting
Rings
(f)
50.0 (mm/d)
Y = 0.016 X
Y = 0.8
Convergence rebound rate (mm/day)
Convergence recovery rate (mm/day)

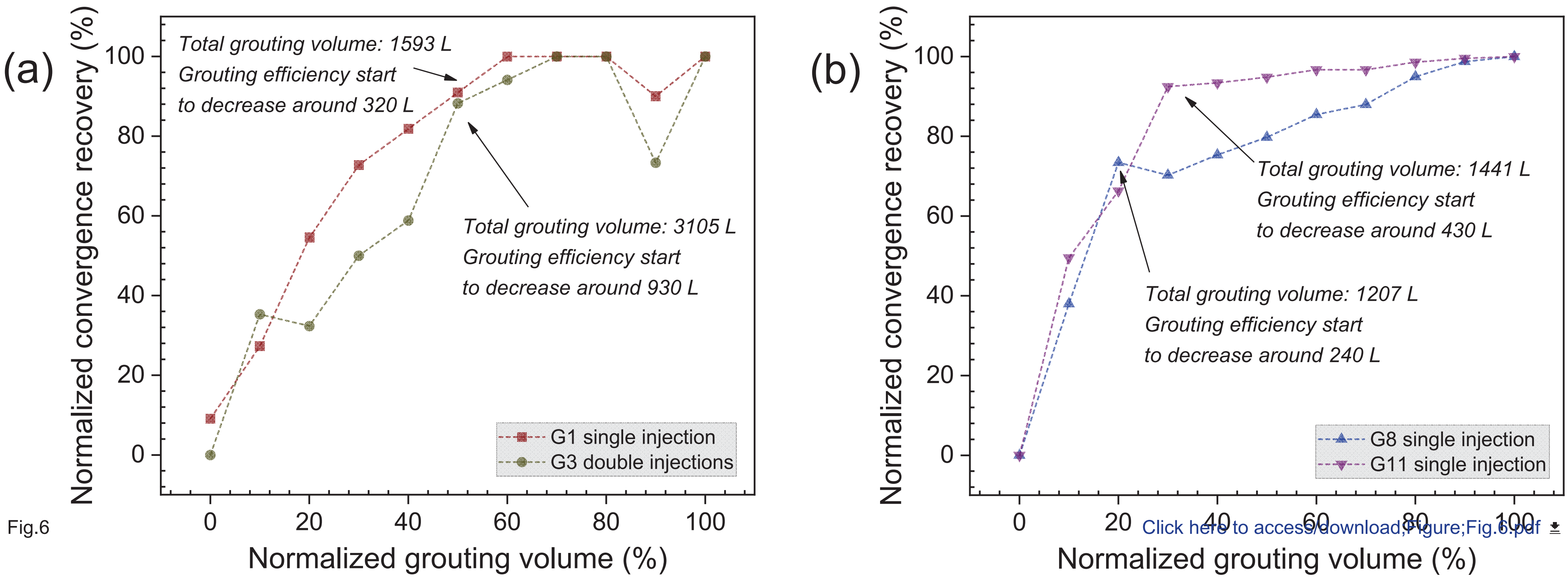
(a)
Normalized convergence recovery (%)
Normalized grouting volume (%)
Total grouting volume: 1593 L
Grouting efficiency start
to decrease around 320 L
Total grouting volume: 3105 L
Grouting efficiency start
to decrease around 930 L
G1 single injection
G3 double injections
(b)
Normalized convergence recovery (%)
Normalized grouting volume (%)
Total grouting volume: 1441 L
Grouting efficiency start
to decrease around 430 L
Total grouting volume: 1207 L
Grouting efficiency start
to decrease around 240 L
G8 single injection
G11 single injection

Fig.6

Click here to access/download;Figure;Fig.7_1.pdf

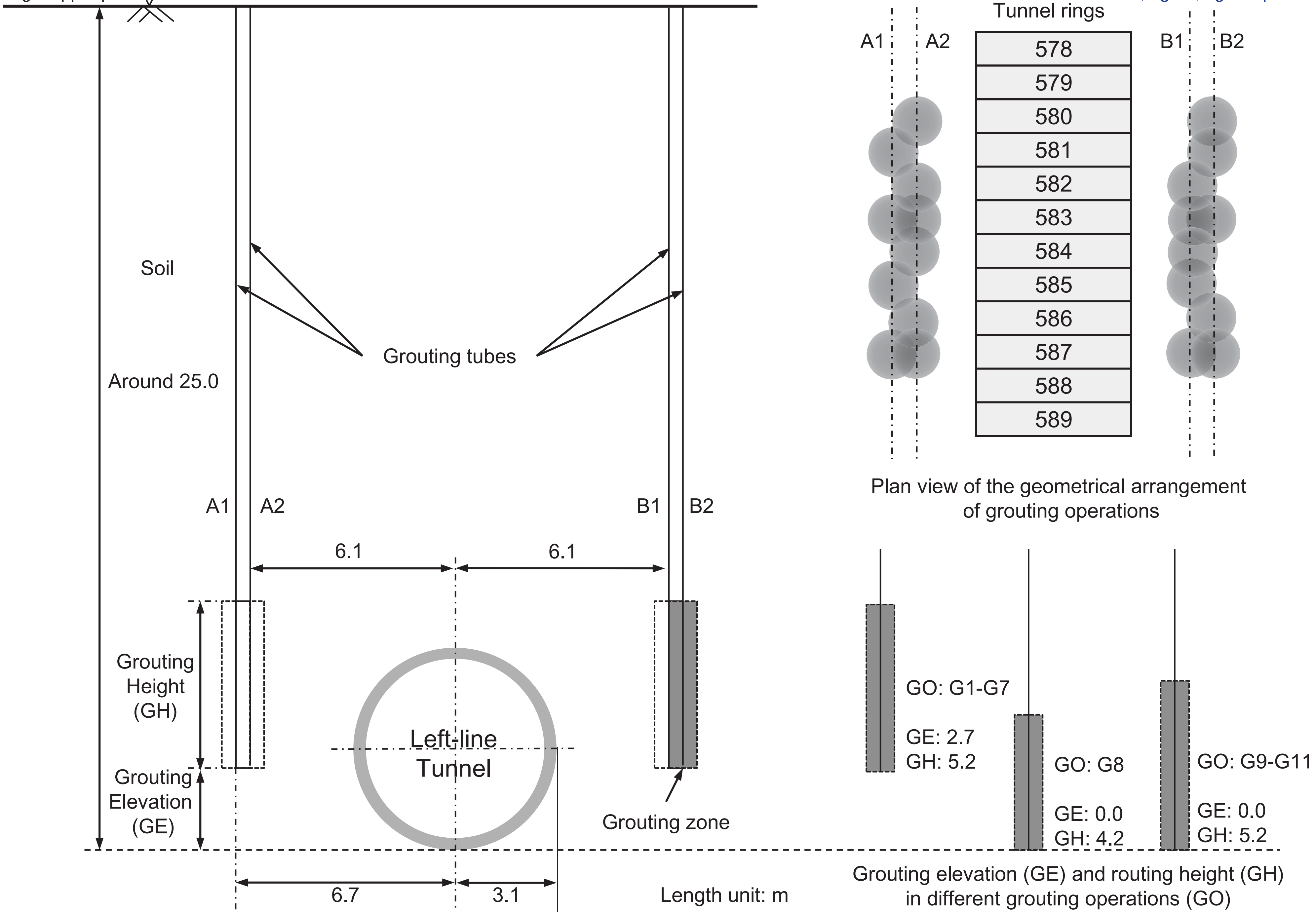

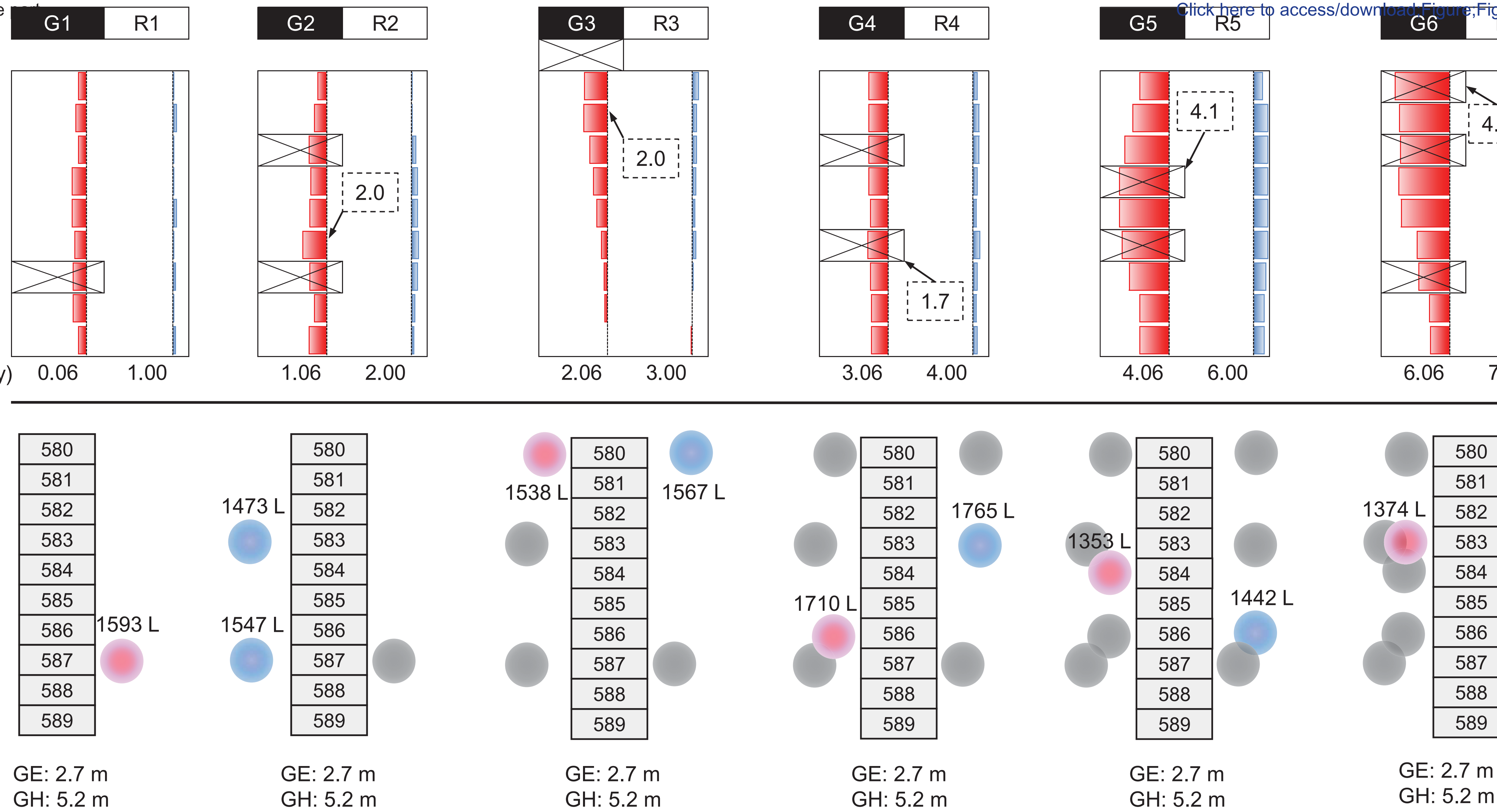
G1
R1
G2
R2
G3
R3
G4
R4
G5
R5
G6
2.0
2.0
1.7
4.1
0.06
1.00
1.06
2.00
2.06
3.00
3.06
4.00
4.06
6.00
6.06
580
581
582
583
584
585
586
587
588
589
1593 L
1473 L
1547 L
1538 L
1567 L
1765 L
1710 L
1353 L
1442 L
1374 L
GE: 2.7 m
GH: 5.2 m

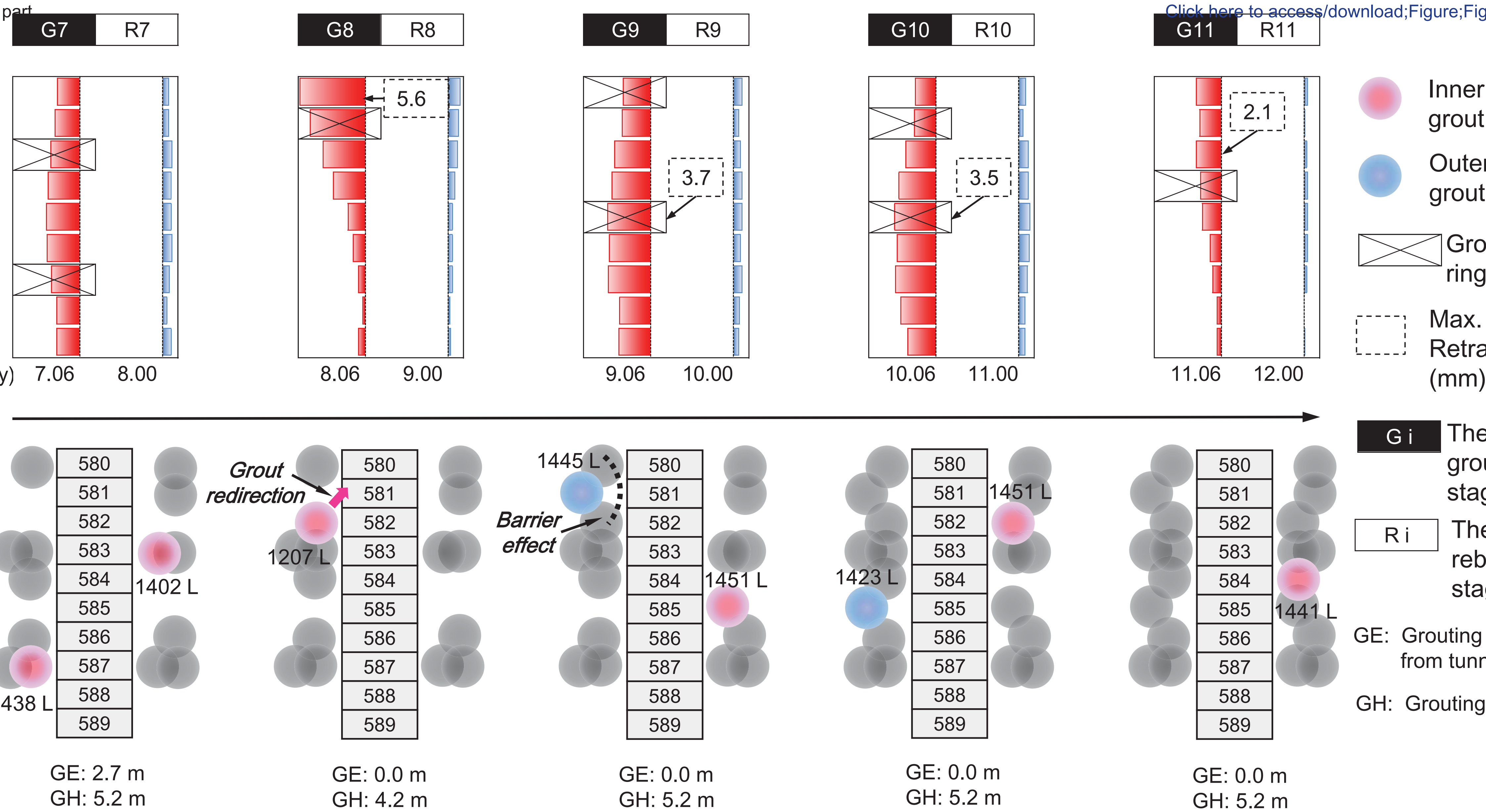
part
G7
R7
G8
R8
G9
R9
G10
R10
G11
R11
5.6
3.7
3.5
2.1
y) 7.06
8.00
8.06
9.00
9.06
10.00
10.06
11.00
11.06
12.00
Inner
grout
Outer
grout
Gro
ring
Max.
Retra
(mm)
G i
The
grou
stag
R i
The
reb
sta
GE: Grouting
from tunn
GH: Grouting
Grout
redirection
Barrier
effect
1445 L
1207 L
1402 L
438 L
1451 L
1451 L
1423 L
1441 L
580
581
582
583
584
585
586
587
588
589
GE: 2.7 m
GH: 5.2 m
GE: 0.0 m
GH: 4.2 m
GE: 0.0 m
GH: 5.2 m
GE: 0.0 m
GH: 5.2 m
GE: 0.0 m
GH: 5.2 m

Fig.8

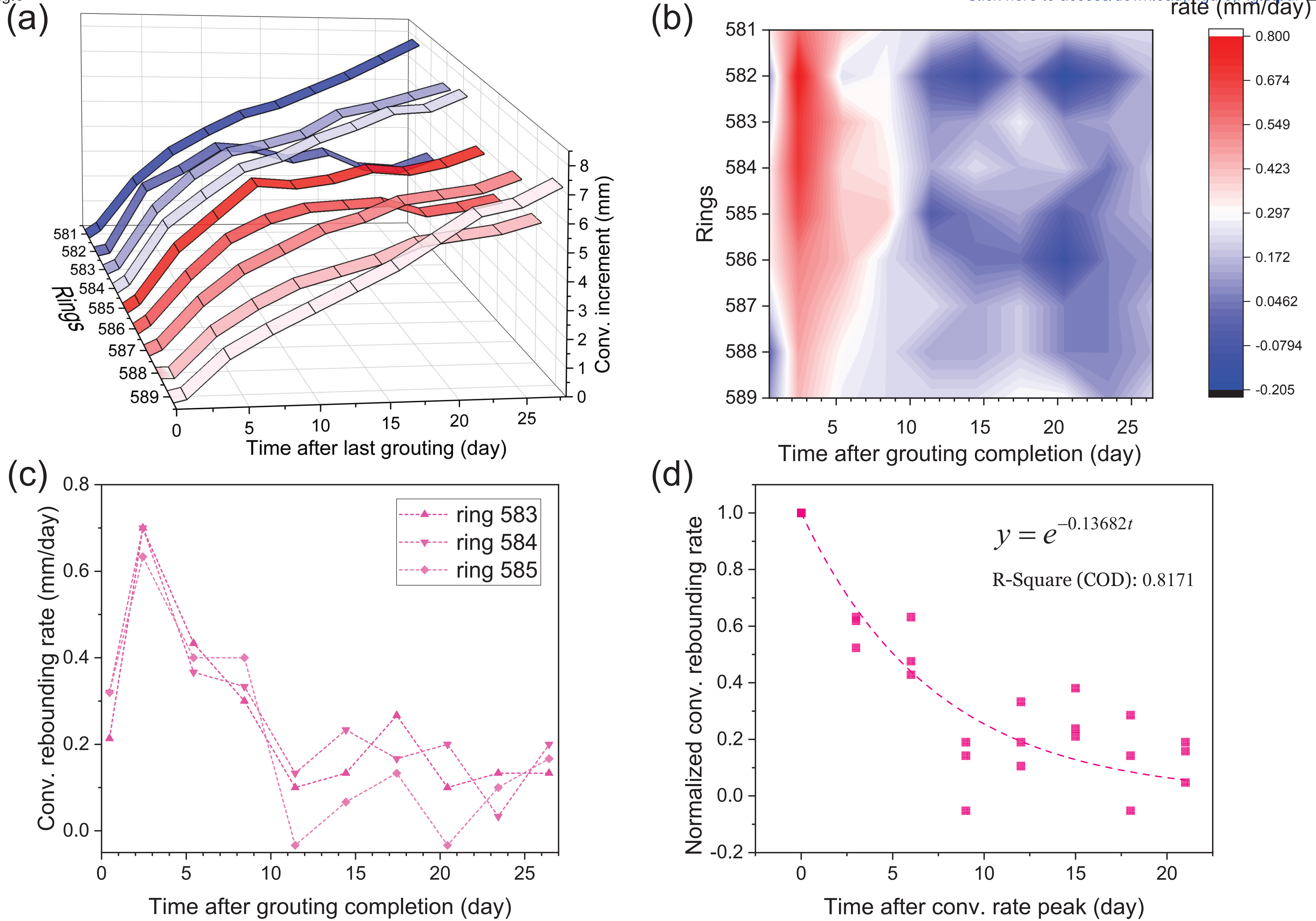

(a)
581
582
583
584
585
586
587
588
589
Rings
0
1
2
3
4
5
6
7
8
Conv. increment (mm)
0
5
10
15
20
25
Time after last grouting (day)
(b)
rate (mm/day)
0.800
0.674
0.549
0.423
0.297
0.172
0.0462
-0.0794
-0.205
Rings
581
582
583
584
585
586
587
588
589
5
10
15
20
25
Time after grouting completion (day)
(c)
Conv. rebounding rate (mm/day)
0.8
0.6
0.4
0.2
0.0
ring 583
ring 584
ring 585
0
5
10
15
20
25
Time after grouting completion (day)
(d)
Normalized conv. rebounding rate
1.0
0.8
0.6
0.4
0.2
0.0
-0.2
$y = e^{-0.13682t}$
R-Square (COD): 0.8171
0
5
10
15
20
Time after conv. rate peak (day)